Ab initio density functional studies of transition-metal sulphides: II. Electronic structure

1997 J. Phys.: Condens. Matter 9 11107

(http://iopscience.iop.org/0953-8984/9/50/014)

J. Phys.: Condens. Matter **9** (1997) 11107–11140. Printed in the UK PII: S0953-8984(97)83863-5

Ab initio density functional studies of transition-metal sulphides: II. Electronic structure

P Raybaud†‡, J Hafner†, G Kresse† and H Toulhoat‡

† Institut für Theoretische Physik and Centre for Computational Materials Science, TU Wien, Wiedner Hauptstraße 8–10, A-1040 Wien, Austria

‡ Institut Français du Pétrole, Groupe de Modélisation Moléculaire, BP 311, F-92852 Rueil-Malmaison, France

Received 30 April 1997, in final form 14 October 1997

Abstract. A study of the electronic structure of about thirty transition-metal sulphides (TMS) of various stoichiometries and crystal structures is presented, supplementing recent studies of their structural and cohesive properties (P Raybaud, G Kresse, J Hafner and H Toulhoat, preceding paper). The electronic structure of the TMS is found to be determined by short-range interactions in the S 3p–TM d band complex, with the ligand-field splitting of the TM d states in the environment of the S atoms determining the structure of the d band. For the layered group VI disulphides, for ReS_2 and for the group VIII pyrites this leads to the formation of a gap at the Fermi surface. Semiconducting properties are predicted also for the monosulphides PtS and PdS and for Rh_2S_3 and Ir_2S_3. We show that the semiconducting TMS have a higher catalytic activity for hydro-desulphurization than the metallic sulphides. We suggest a correlation between the catalytic activity and the characters of the highest occupied states (the frontier orbitals).

1. Introduction

In the preceding paper of this series (hereafter referred to as I) [1] we have presented a comprehensive investigation of the structural and cohesive properties of more than thirty transition-metal sulphides (TMS) within the local density approximation (LDA) [2, 3]. We have shown that for most sulphides there is a quite pronounced trend towards an overbinding which manifests itself in the prediction of too small atomic volumes and too large cohesive energies. Non-local corrections to the LDA in the form of a generalized-gradient approximation (GGA) [4] correct for the overbinding (albeit with a certain tendency for the sulphides of the heavier transition metals to overcorrect the LDA error) and lead to accurate crystal structures and cohesive energies. We have also demonstrated that there is a clear correlation between the cohesive energies calculated in the LDA + GGA and the catalytic activities of the TMS in hydro-desulphurization processes. In this paper we supplement these investigations with a comprehensive study of the electronic structure of the TMS.

The layered TM disulphides belong to a family of structures consisting of different stacking variants of tightly bound two-dimensional S–TM–S sandwiches. Depending on the relative arrangement of the two S layers, the coordination of the TM atoms by six S atoms is trigonal prismatic or octahedral. Early band-structure calculations [5–7] demonstrated that the electronic structure is determined by the combined effects of the ligand-field splitting of the d levels in the trigonal-prismatic surrounding and the d–d hybridization of the Mo 4d

0953-8984/97/5011107+34$19.50

states. Huisman *et al* [6] demonstrated that due to the ligand-field splitting a two-electron band of mainly $d_{3z^2-r^2}$ character is separated from the main part of the TM d band and hybridizes strongly with the S p band. The trigonal-prismatic coordination is stabilized with respect to the octahedral coordination for disulphides with d^1 or d^2 configurations. More advanced band-structure calculations confirmed this picture [8–11].

In the cubic pyrite structure and the closely related marcasite structure, each TM atom is again surrounded by six nearest-neighbour sulphur atoms in a distorted octahedral environment while each S atom sits at the centre of a distorted tetrahedron formed by one S and three TM atoms. The S–S pairs are a characteristic feature of both structures. Electronic structure calculations for this class of compounds have first been performed by Li *et al* [12], Tossel *et al* [13], Khan [14] and Bullett [15]. The main characteristics of the electronic band structure may be derived from the assumption that the sulphur pairs may be considered as divalent molecular anions, S_2^{2-}, with empty antibonding $p\sigma^\star$ states. In the distorted octahedral surrounding, the TM d band splits into t_{2g} and e_g manifolds. Hence FeS_2 will be a semiconductor with the Fermi level in the t_{2g}–e_g gap, while the compounds with a higher degree of filling of the d band are expected to be metallic up to ZnS_2. In fact CoS_2 is a ferromagnetic metal, while NiS_2 is an antiferromagnetic Mott–Hubbard insulator and becomes metallic only under pressure [16]. The general picture of the electronic structure of pyrite compounds has been confirmed by more recent band-structure calculations [17–23] and various spectroscopic studies [20, 23–25].

In this paper we shall concentrate on the trends in the electronic structure of both layered and cubic disulphides with increasing filling of the d band, and the relation of these trends to the relative stability of both types of structure. Our investigations also include the distorted ReS_2-type and marcasite-type structures appearing at the limits of the stability ranges of both classes of compound.

The electronic structure of the hexagonal NiAs-type transition-metal monosulphides has been investigated mainly from the point of view of the magnetic properties of the 3d monochalcogenides and the isostructural pnictide compounds [27, 28]. Schematic band-structure models based on ligand-field arguments have been proposed by White and Mott [29] and Wilson [30]. The thermodynamically stable low-temperature phases, however, have either low-symmetry structures (FeS: troilite (complex superstructure of NiAs); NiS: trigonal millerite) or off-stoichiometric phases like Co_9S_8. The pioneering band-structure calculations for NiAs-type compounds (mostly for NiS) by Tyler and Fry [31], Mattheis [32], and Kasowski [33] point to a predominantly ionic band structure. The more recent band-structure studies of Motizuki *et al* [34] and Dijkstra *et al* [35] emphasize the importance of TM–TM interactions along the hexagonal axis; see also the related work on the pnictide compounds [36, 37]. Recent work by Fujimori *et al* [38, 39] has challenged the interpretation of NiS as a Mott–Hubbard insulator and led to the proposal of an alternative explanation in terms of a S 3p–Ni 3d charge-transfer gap.

In the present work we shall extend the investigations to the complete series of 3d monosulphides and some of the 4d compounds. At the end of all three transition-metal series, monosulphides with different structures (tetragonal PdS and PtS, trigonal NiS (millerite)) and slightly off-stoichiometric compounds (cubic Co_9S_8) are stabilized. We discuss the stability of these compounds in relation to their electronic structure. We also include some TMS of composition intermediate between the monosulphides and disulphides and some substoichiometric sulphides in our investigations (Rh_2S_3, Ir_2S_3, Ni_3S_2). Finally we return to the correlation between the electronic spectrum and the catalytic activity of the TMS.

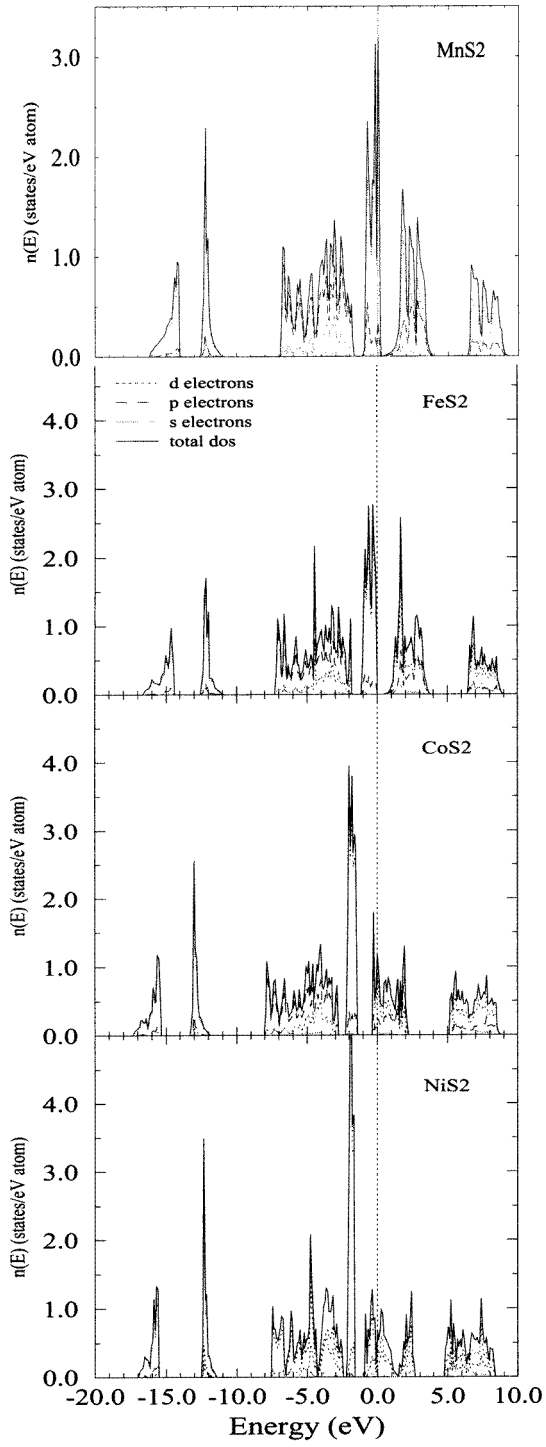

Figure 1. Total and angular-momentum-decomposed electronic densities of states of the pyrite-type compounds MnS_2, FeS_2, CoS_2 and NiS_2. Full line: total DOS; dotted, dashed, chain lines: s, p, d partial DOSs.

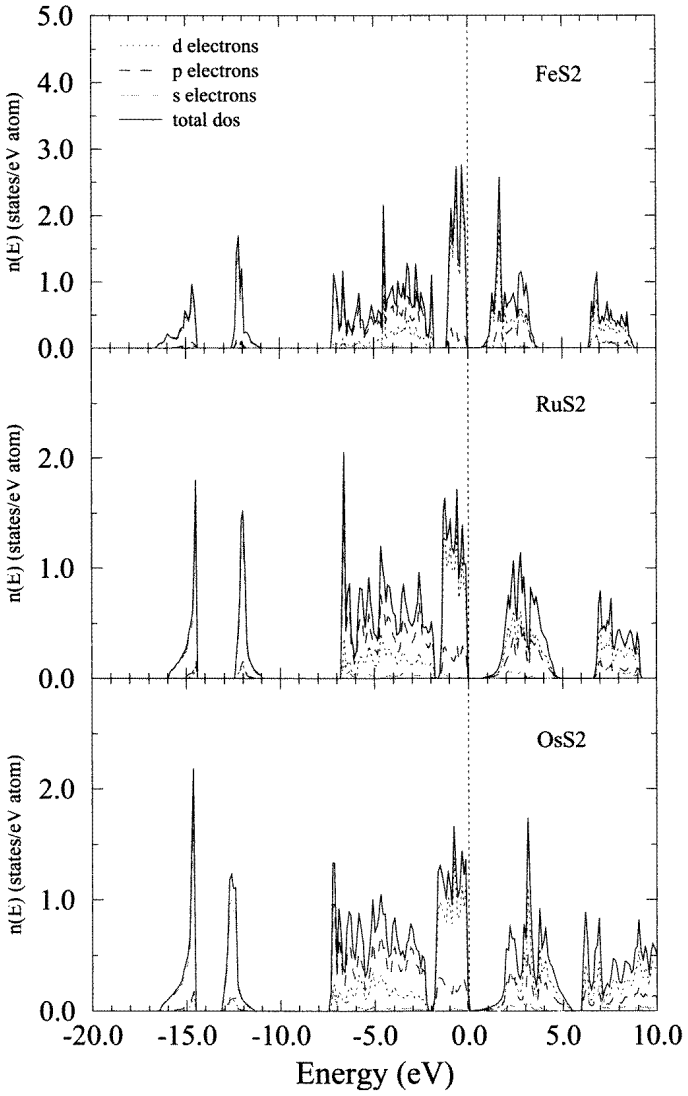

Figure 2. Total and angular-momentum-decomposed electronic densities of states of the FeS_2, RuS_2 and OsS_2 pyrites. The key to the curves is the same as in figure 1.

2. Computational aspects

Our electronic structure calculations have been performed using the Vienna *ab initio* simulation program VASP. The most important aspects of the technique have been briefly described in I; for all technical aspects we refer the reader to the papers by Kresse and Furthmüller [40].

We emphasize that the electronic structure has been calculated for the equilibrium structure determined from the LDA + GGA calculation and not for the experimentally determined structure. Hence our calculations represent the true ground state as given by density functional theory and documented in I.

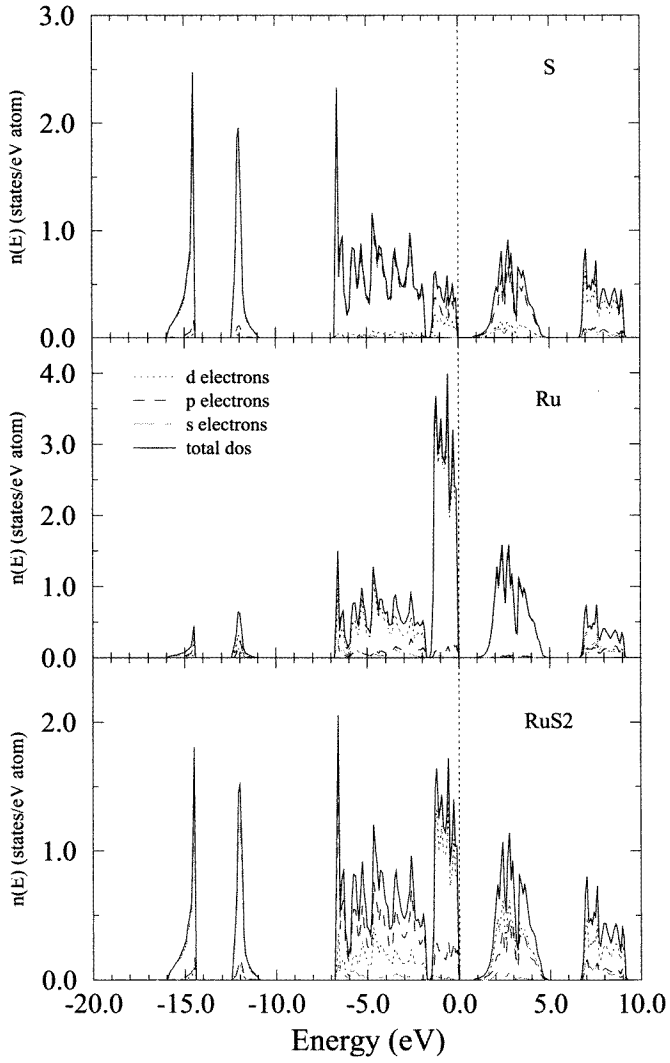

Figure 3. Total and local Ru and S densities of states in RuS_2, decomposed into angular-momentum components. The key to the curves is the same as in figure 1.

3. Electronic structure of the transition-metal disulphides

3.1. Pyrite-type compounds

The total and angular-momentum-decomposed electronic densities of states (DOS) of the pyrite-type compounds MnS_2, FeS_2, CoS_2 and NiS_2 with an increasing filling of the d band are represented in figure 1. The variation of the DOS in a homologous series of compounds is shown in figure 2 for an example of the series: FeS_2–RuS_2–OsS_2. For RuS_2 we present in addition the decomposition of the DOS into the transition-metal and sulphur contributions (figure 3).

The valence bands plus the lowest conduction bands form six groups neatly separated

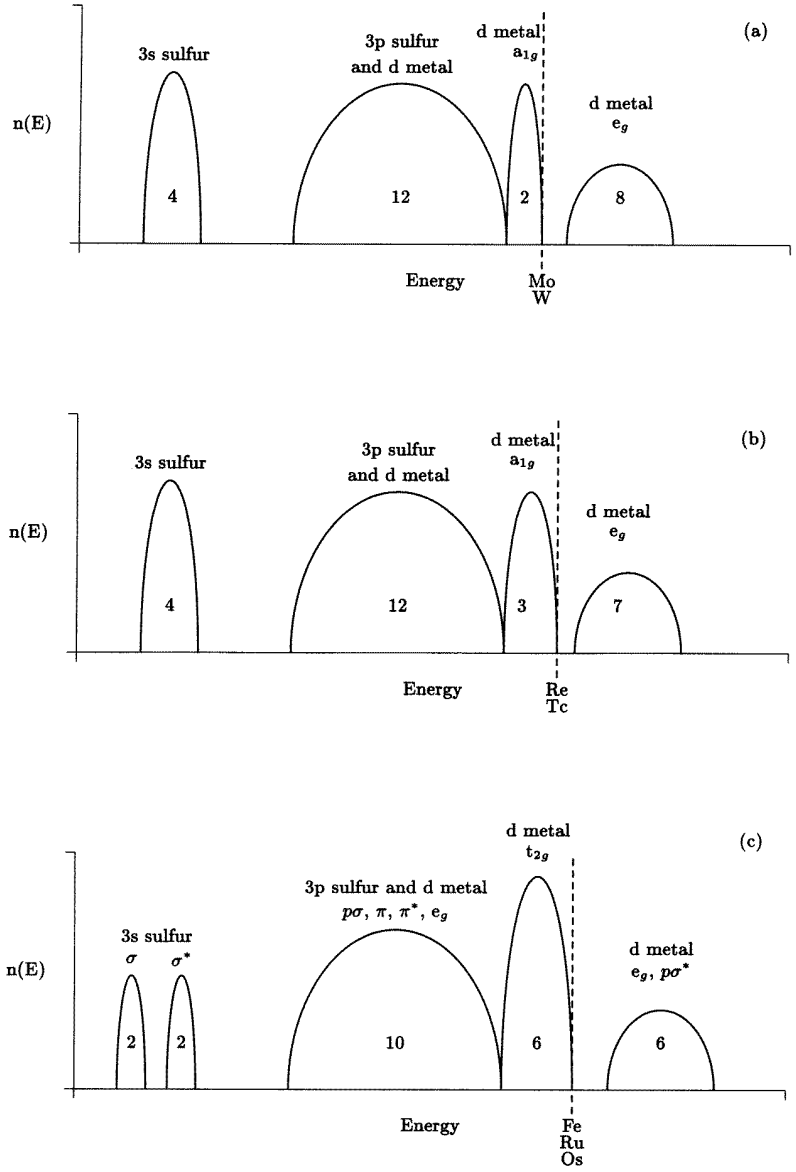

Figure 4. A schematic model for the electronic band structures of transition-metal disulphides in different crystal structures. (a) MoS_2-type layered structure: S s band/S p band/TM $a_{1g}(d_{3z^2-r^2})$ band (two electrons)/TM ($d_{t_{2g}} + d_{x^2-y^2}$) bands. (b) ReS_2 structure: S s band/S p band/TM a_{1g} band/TM e_g band. (c) Pyrite structure: bonding and antibonding S σ and $\sigma^\star$ bands/S $p\sigma$, $p\pi$, $p\pi^\star$ states hybridized with TM e_g states/TM t_{2g} band/antibonding TM $e_g^\star$ and S $p\sigma^\star$ bands. The position of the Fermi level in sulphides of transition metals from groups Vb (a), VIIb (b), and VIIIb (c) is indicated.

by narrow gaps. Since there are four formula units in each elementary cell, for FeS_2, RuS_2 and OsS_2 the occupied bands must accommodate $4(8+2\times 6) = 80$ valence electrons. This corresponds to a complete filling of the first four groups of bands, so the pyrites of the Fe

group are narrow-gap semiconductors with a gap varying between $E_g = 0.38$ eV in FeS_2, $E_g = 0.56$ eV in RuS_2 and $E_g = 0.11$ eV in OsS_2; the other pyrites are metallic due to an incomplete filling of the fourth or fifth group of bands. The experimentally determined optical gaps are $E_g = 0.95$ eV (reference [41]) and $E_g = 1.15$ eV (reference [42]) for RuS_2 as determined from single-crystal data. The underestimation of the gap width reflects the fact that the LDA is a ground-state theory and cannot rigorously be used to study excited states—this problem is not solved by the GGA.

The rigidity of the pyrite band structure reflects the dominant influence of short-range interactions, as discussed in the literature [13, 15, 19]. These short-range interactions can be described to a first approximation in terms of crystalline eigenstates derived from S_2^{2-} molecular orbitals and from the TM d orbitals split in the octahedral crystal field. The S $3s\sigma$ and $3s\sigma^\star$ states form the two narrow bands centred at $E \sim -15$ eV and $E \sim -12$ eV, respectively. The S 3p states are split into four groups of bands. The bands extending in RuS_2 from -6.8 eV to -1.6 eV can be associated with the S $3p\sigma$, $3p\pi$ and $3p\pi^\star$ states, while the antibonding $3p\sigma^\star$ states are shifted above the Fermi level. The TM atoms are located in an octahedral environment of S atoms (slightly trigonally distorted). In the octahedral crystal field the fivefold-degenerate TM d orbitals split into the threefold-degenerate t_{2g} (d_{xy}, d_{yz}, d_{xz} in the coordinate system oriented along the cubic axes) and the twofold-degenerate e_g ($d_{x^2-y^2}$, $d_{3z^2-r^2}$) orbitals. The t_{2g} orbitals are oriented away from the TM–S bonding directions, so they are essentially non-bonding. These levels form the groups of 12 narrow bands just below the Fermi level in FeS_2 and RuS_2. The e_g orbitals extend along the direction of the TM–S bonds and hybridize strongly with the S 3p states. This hybridization occurs in such a way that the bonding TM e_g–S 3p levels form a group of 20 bands just below the non-bonding t_{2g} bands, in exact correspondence to the 20 bands that could be formed by the S $3p\sigma$, $3p\pi$ and $3p\pi^\star$ levels alone. The antibonding TM e_g–S 3p hybrids form a set of 12 bands (four from the S $3p\sigma^\star$ states and eight from the TM e_g states) above the t_{2g} bands, separated by a narrow gap of a few tenths of an eV. A schematic sketch of the pyrite band structure is given in figure 4(c).

This general form of the band structure does not change appreciably with the number of d electrons contributed by the TM (figure 1): as we go from MnS_2 to NiS_2, the width of the bonding and antibonding TM e_g–S 3p complexes is nearly unchanged; the non-bonding TM t_{2g} band narrows because of the more strongly localized TM 3d states. Within the isoelectronic series FeS_2–RuS_2–OsS_2 the main effect is a broadening of the t_{2g} band arising from the increasing spatial extension of 4d and 5d orbitals.

X-ray photoemission spectra have been taken for RuS_2 by Kuhne *et al* [18], van der Heide *et al* [43] and Lauer *et al* [17] for FeS_2, CoS_2 and NiS_2; the structure of the conduction band has been probed for FeS_2, CoS_2 and NiS_2 by inverse photoemission experiments [20, 25]. Figure 5 demonstrates the very good correspondence of the positions and widths of the occupied S 3p and Fe 3d (t_{2g}) bands and of the empty Fe 3d(e_g), S $3p\sigma^\star$ and Fe 4sp–S 3d bands. A similarly good agreement is also found between the XPS data of Kuhne *et al* [18] and the calculated DOS for RuS_2: a strong emission peaked at -1.2 eV below E_F corresponds to the Ru 4d (t_{2g}) states; structures between -2 eV and -7 eV can be associated with details of the S $3p\sigma$, $3p\pi$, $3p\pi^\star$ band (see figure 3). Emission peaks at about -12.9 eV correspond to the S $3s\sigma$ and $\sigma^\star$ bands. Compared to the calculated band positions, the emission peaks are shifted to higher binding energies due to self-energy corrections of the order of 1 eV. These corrections are characteristic for photoemission spectra for narrow bands.

For CoS_2 the DOS at the Fermi level ($n(E_F) = 1.25$ states eV^{-1}/atom; see figure 1) is sufficiently high that according to the Stoner model the paramagnetic state is unstable against

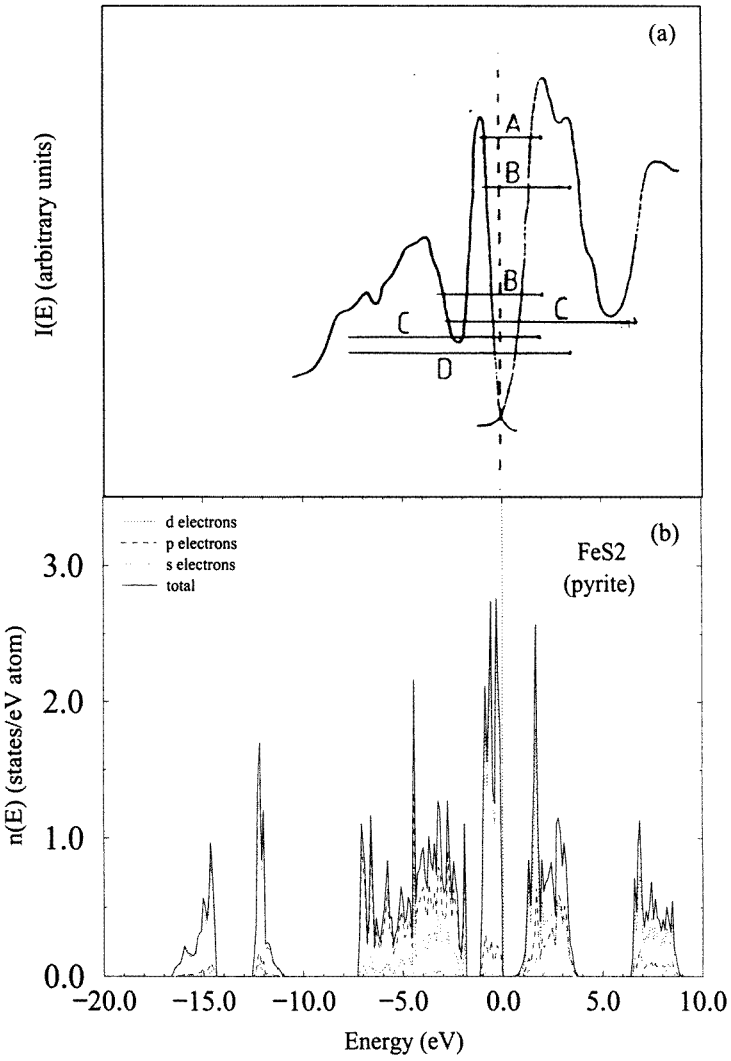

Figure 5. Comparison of the total density of states of FeS_2 pyrite (a) with the x-ray photoemission and inverse photoemission spectra of Folkerts *et al* (reference [20]) (b). The transitions labelled A to D correspond to the main peaks in the measured optical adsorption and electron-energy-loss spectra. See the text.

the formation of a magnetic moment. Indeed CoS_2 is a ferromagnetic metal with a small magnetic moment ($0.8\mu_B$ per Co atom; reference [46]). The photoemission spectra recently taken by Fujimori *et al* [45] show a broadening of the characteristic t_{2g} peak about -1.6 eV below the Fermi level compared to FeS_2 and a less distinct S 3p–Co t_{2g} separation. The broadening of the t_{2g} peak must be interpreted as resulting from the exchange splitting that persists on the short timescale of the photoemission experiment even in the paramagnetic state as proposed in a local band picture [47]. The exchange splitting also leads to a broadening of the Co d(e_g) band observed via IPES (reference [25]). The IPES spectra also confirm the onset of the Co 4sp–S 3d band at 5 eV (cf. figure 1).

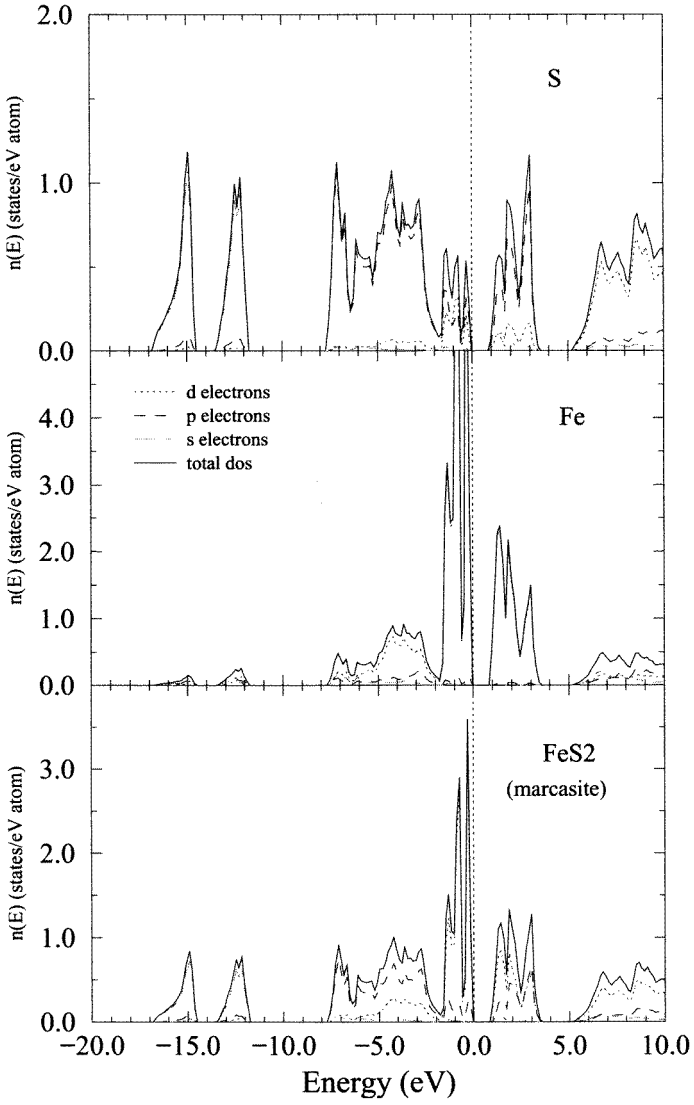

Figure 6. Total and local Fe and S (angular-momentum-decomposed) densities of states in FeS_2 marcasite (the key to the curves is the same as in figure 1).

For NiS_2 the band calculations predict a metallic behaviour, albeit with the Fermi level within a DOS minimum in the middle of the Ni d(e_g) band which is now distinctly separated from the empty S 3p$\sigma^\star$ band. However, correlation effects lead to the formation of a gap at the Fermi level, but there is still some debate about whether the gap is of the Mott–Hubbard d–d type [5, 48] or a charge-transfer p–d gap [44, 45].

3.2. Marcasite FeS_2

In the orthorhombic marcasite structure the characteristic distorted octahedral cation units share edges (and not only corners like in the pyrite structure), forming chains along the

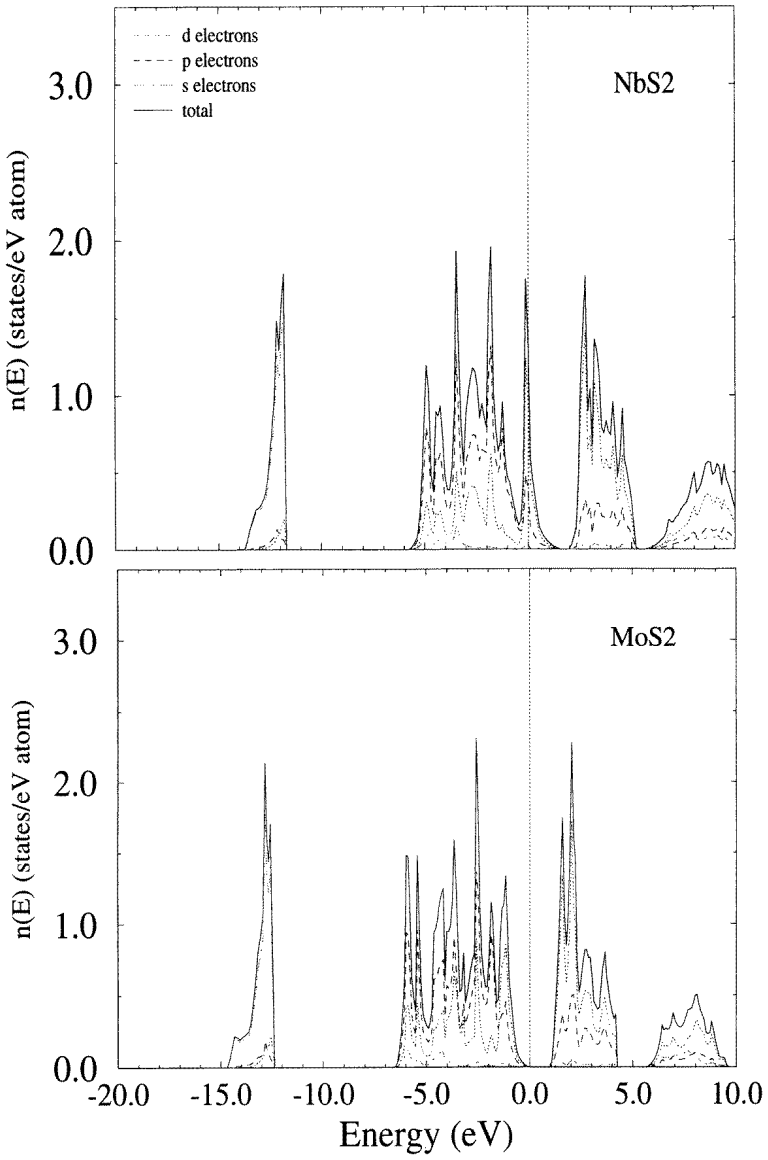

Figure 7. Total and angular-momentum-decomposed densities of states of the layered disulphides NbS_2 and MoS_2 (the key to the curves is the same as in figure 1).

orthorhombic *c*-direction. The stronger distortion of the octahedral environment and the Fe–Fe interactions across the triangular faces lead to a splitting of the t_{2g} bands (figure 6). The S 3s and 3p bands are slightly broadened relative to the pyrite structure; the S 3p bands now overlap with the lower edge of the t_{2g} band. The width of the optical gap is increased from $E_g = 0.38$ eV in the pyrite structure to $E_g = 0.58$ eV in the marcasite structure. This is a consequence of the increased bonding–antibonding splitting in the Fe e_g–S $3p\sigma$ band complex resulting from stronger Fe–Fe interactions. The 20 meV/atom energy gain relative to the pyrite form (cf. I) can be attributed to the improved metal–metal bonding.

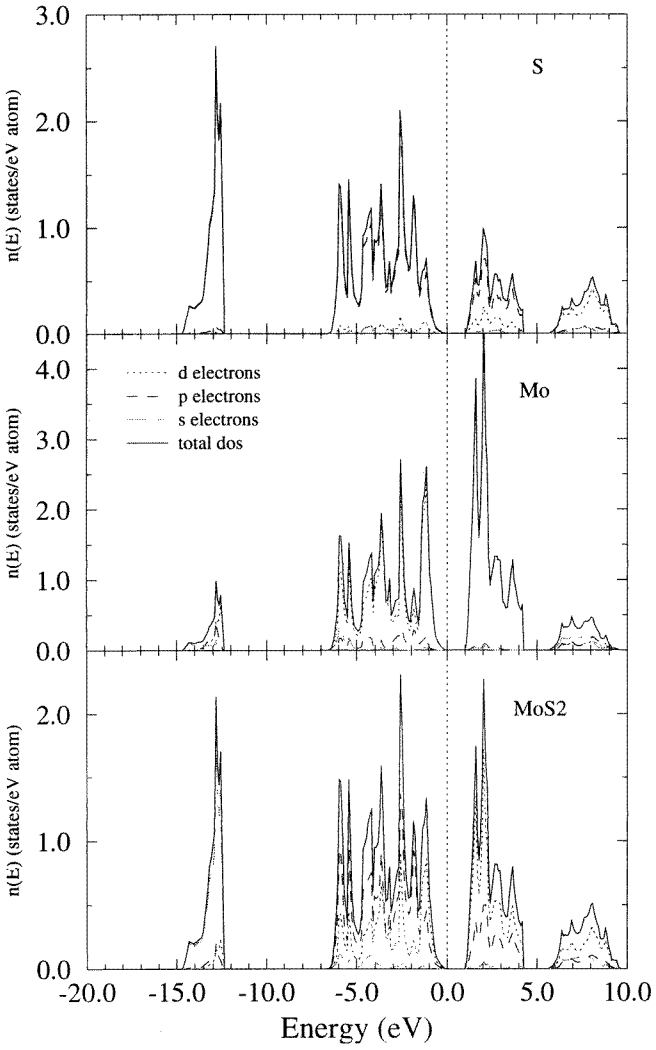

Figure 8. Total, local and partial Mo and S densities of states for MoS_2 (the key to the curves is the same as in figure 1).

3.3. Layered MoS_2-type disulphides

The layered dichalcogenides of the group IVb, Vb and VIb transition elements form a class of structures for which the coordination of the metal atom is either trigonal-prismatic (e.g. NbS_2, MoS_2, TaS_2, WS_2), or octahedral (e.g. the Ti, Zr, Hf and V dichalcogenides and a second polymorph of TaS_2). Figure 7 shows the total and angular-momentum-decomposed DOSs for NbS_2 and MoS_2; figure 8 presents in addition the local Mo and S DOSs for MoS_2. MoS_2 is found to be semiconducting with a gap of $E_g = 0.89$ eV, while NbS_2 is found to be metallic with a sharply peaked DOS at the Fermi level. The band structures of the homologous 5d compounds show no characteristic differences; WS_2 is semiconducting with an optical gap of $E_g = 0.91$ eV.

Our results confirm the interpretation of the electronic structure given on the basis of

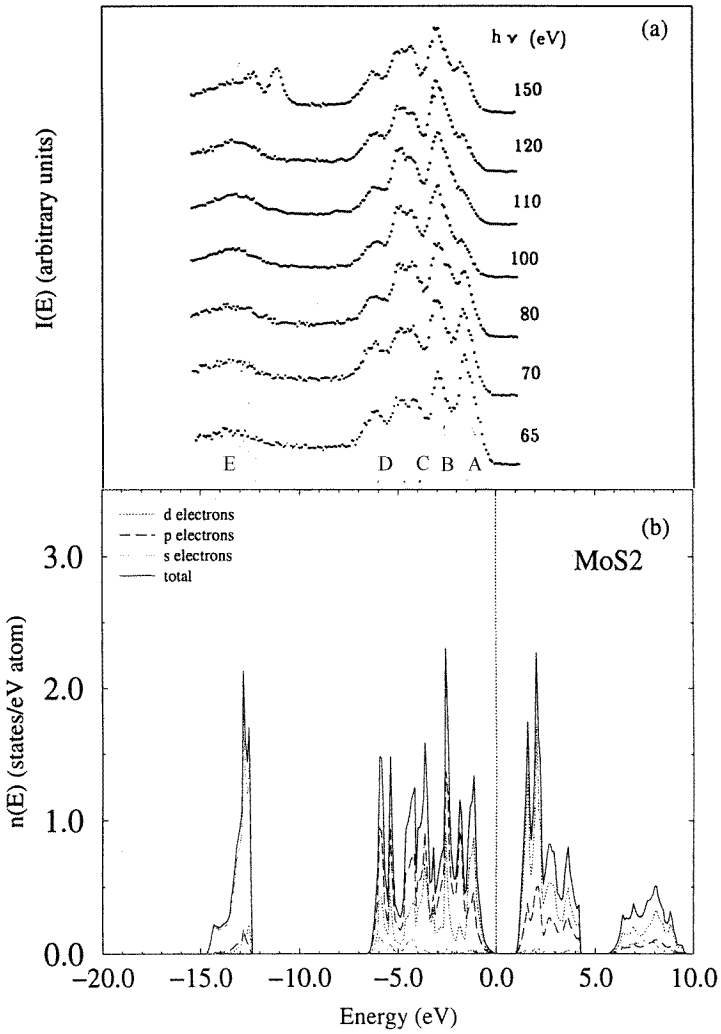

Figure 9. Comparison of the photoemission spectra (a) measured by Abbati *et al* (reference [50]) at various photon energies with the theoretical DOS (b). The emission peaks labelled A to E can be attributed to (A) the Mo a_{1g} band, (B to D) the S 3p band and (E) the S 3s band. See the text.

the ligand-field splitting of TM d states, resulting from the covalent TM d–S p bonding rather than from a crystal-field effect [6–11]. Since the D^3_{3d} and D^4_{6h} space groups of the octahedral and trigonal-prismatic layer structures contain a unique z-axis, the S p states subdivide into two groups (p_z and p_x, p_y) and the TM d states into three groups ($d_{3z^2-r^2}$; d_{xy} and $d_{x^2-y^2}$; d_{xz} and d_{yz}). An octahedral ligand field splits the d level into triply degenerate t_{2g} ($d_{3z^2-r^2}$, d_{xy}, $d_{x^2-y^2}$ in the coordinate system with the z-axis oriented along the hexagonal (trigonal) axis) and doubly degenerate e_g (d_{xz}, d_{yz}) sets. Under a trigonal distortion the t_{2g} set splits into a non-degenerate a_{1g} and doubly degenerate e_g sets (see also the discussion of the electronic structure of marcasite). In a trigonal ligand field the t^0_{2g} wave function is equivalent to the non-degenerate a_{1g}. It is dominated by the $d_{3z^2-r^2}$ wave function and has

the lowest energy. The t_{2g}^{+} and t_{2g}^{-} wave functions correspond to the doubly degenerate e_g state split from the t_{2g} set and mix with the other e_g set [49]. Assuming an essentially ionic charge state we arrive at the band structure sketched in figure 4(a). The lowest group of bands corresponds to the completely filled S 3s states. A full S 3p band overlaps with the TM a_{1g} band dominated by the TM $d_{3z^2-r^2}$ states. For MoS_2 and WS_2 the Fermi level falls at the upper edge of the a_{1g} band; for NbS_2 and TaS_2 the a_{1g} band is half-filled. The e_g band complex forms the lowest groups of conduction bands. This schematic model shows good agreement with our band calculations, but we also note an appreciable TM e_g/S p mixing.

In figure 9 we compare the calculated DOS for MoS_2 with the photoemission spectra taken by Abbati *et al* [50] with synchrotron radiation at various photon energies. We note an excellent correspondence between the principal emission features labelled A to E and the main peaks in the theoretical DOS. The measured spectra show a strong dependence on the photon energies, arising mainly from the presence of a Cooper minimum [51] in the photoionization cross-section of the Mo 4d states [52, 53] at energies of $\hbar\omega \sim 100$ eV. This allows one to associate peak A with the Mo a_{1g} band. However, since the ratio of the photoionization cross-sections of the S 3p and Mo 5s states to that of the S 3s state remains approximately constant whereas the relative intensity of the peaks B to E varies with the energy of the incident photons, we conclude that there is an appreciable admixture of Mo 4d character to the S 3p band—in agreement with the theoretical DOS.

Further confirmation of the calculated band structure comes from the analysis of the x-ray emission (XES) and x-ray adsorption near-edge structure (XANES) spectra (see figure 10) reflecting the partial DOS of the corresponding valence-band states: the S $L_{2,3}$M spectrum corresponds to the S 3s band, the S $K_{\beta_{1,3}}$ spectrum to the S 3p band and the Mo $L_{\beta_{2,15}}$ and Mo 5p $3d_{5/2}$ spectra to the Mo 4d and Mo 5p states (experimental data from Šimunek and Wiech [54] and Haycock *et al* [55] as collected by Li *et al* [56]). All of the XES spectra have been aligned with the UPS spectra of Abbati *et al* [50]. The S K- and S L-edge XANES features are attributed to transitions of S 1s and S 2p electrons to the unoccupied p and s, d states at S sites. The Mo L_3- and L_2-edge XANES spectra are assigned to transitions of Mo $2p_{3/2}$ and Mo $2p_{1/2}$ electrons, respectively, to the empty Mo 4d states. Again this assignment is in very good agreement with the calculated partial DOS.

3.4. ReS_2

A rigid-band picture applied to the group VIIb disulphides would predict a metallic behaviour in either the layered or the pyrite structure (see figure 11). Our calculations presented in I have shown that at the band filling of the group VIIb metals, the two structures are energetically almost degenerate in all three TM rows. Experimentally, an optical gap of 1.33 eV has been found for ReS_2 (a slightly narrower gap of 1.15 eV exists also in $ReSe_2$) [5, 57]. The formation of a semiconducting gap is due to the formation of triclinic low-symmetry structures in ReS_2 and in the isoelectronic compounds TcS_2 and $ReSe_2$ (see table 1 in I for detailed references).

These triclinic structures can be considered as arising from a deformation of the octahedral stacking variants of the layered disulphide structures. The situation is to some extent similar to that for the group Vb disulphides in which both the octahedral and the trigonal-prismatic polymorphs show charge-density-wave instabilities resulting in phonon softening and the formation of incommensurate phases [5, 58]. For ReS_2 it has been shown that the triclinic structure may be derived from the octahedral layered structure by a shift of the Re atoms such as to form approximate Re_4 units in the central plane of the S–TM–S sandwich [59]. The consequences of this distortion for the electronic structure have been

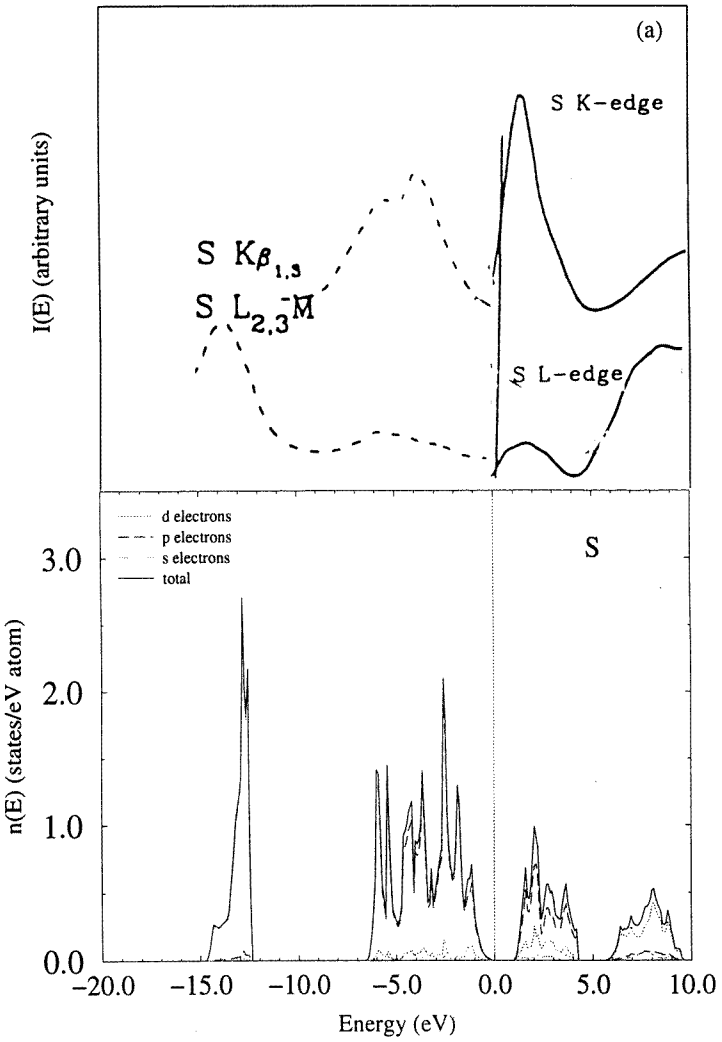

Figure 10. (a) Comparison of the S XES (dashed lines) and S XANES spectra (full lines) with the partial S DOS in MoS_2. (b) Comparison of the Mo XES (dashed lines) and Mo XANES spectra (full lines) with the partial Mo DOS in MoS_2. Experimental data from Li *et al*, reference [56].

discussed by Kertesz and Hoffmann [10] in terms of ligand-field arguments and extended Hückel calculations. The essential point is that in the trigonal-prismatic environment the $d_{3z^2-r^2}$ states are lowered with respect to the remaining d_{xy} and $d_{x^2-y^2}$ states in the t_{2g} triplet. If the $d_{3z^2-r^2}$-derived band is filled by the two d electrons of the group VIb ions, the trigonal-prismatic arrangement is stabilized, whereas for the group Vb disulphides with a half-filled band the two polytypes are of comparable stability. In the group VIIb disulphides the t_{2g} band complex would be just half-filled in an octahedral coordination. Hence the energy can be lowered by forming a gap in the middle of it, i.e. the ratio of bonding and antibonding regions (corresponding to short and long bonds) should be 1:1. For a lattice derived from hexagonal structure this cannot be realized by a simple doubling of the unit cell, but requires

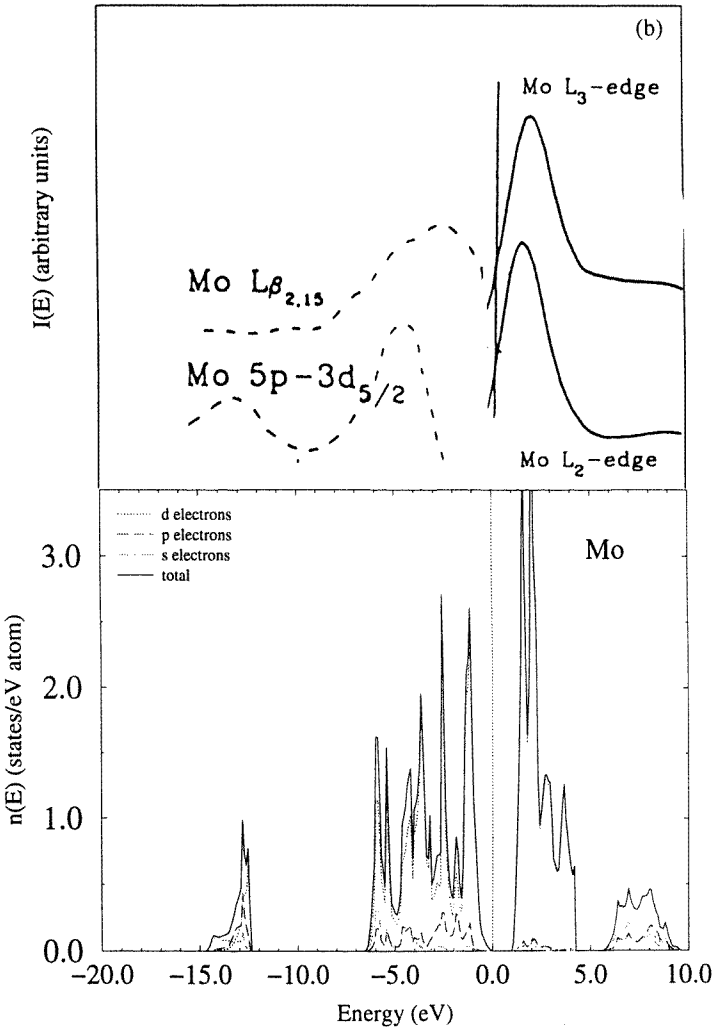

Figure 10. (Continued)

four units. This is realized in the ReS_2 structure with its characteristic Re_4 units.

The total and partial DOSs for ReS_2 shown in figure 12 demonstrate the existence of a gap of $E_g \sim 1.16$ eV, in good agreement with the experimental observation. The structural energy difference relative to the energetically degenerate MoS_2 and FeS_2 structures is 0.31 eV/atom (cf. section 5.1 in I, but remember that we did not consider the undistorted octahedral layer structure). The bonding t_{2g} band overlaps strongly with the S 3p band; the antibonding t_{2g} band overlaps with the Re e_g band.

3.5. Electronic structure and structural trends

In I we have shown that total energy calculations in the LDA + GGA correctly predict the change in the relative stability of the layered and pyrite-type disulphides with increasing

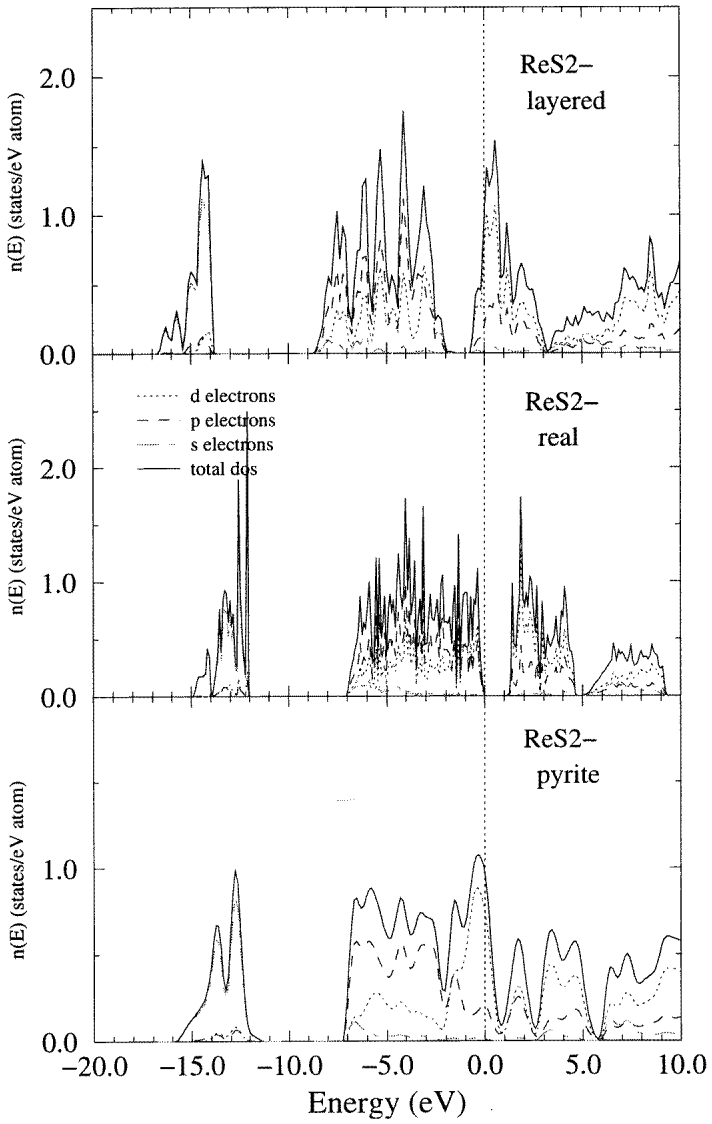

Figure 11. The total electronic density of states for ReS_2 in the layered MoS_2-, triclinic and pyrite structures (the key to the curves is the same as in figure 1).

filling of the transition-metal d band. We are now in a position to relate this trend to the details of the electronic structure. The guiding principle is the formation of a strong covalent bond in the S 3p–TM d band complex, associated with the formation of a semiconducting gap at the Fermi level. For low band filling this is most easily achieved by forming a fully occupied non-bonding $d_{3z^2-r^2}$ band as in the trigonal layered structure; at high band filling optimal stabilities are achieved for a completely filled (again non-bonding) t_{2g} band complex formed in the cubic pyrites. Partial filling of either band leads to various structural instabilities: trigonal/octahedral polytypism and charge-density-wave instabilities in the layered group Vb disulphides, formation of the distorted ReS_2 structure in the VIIb

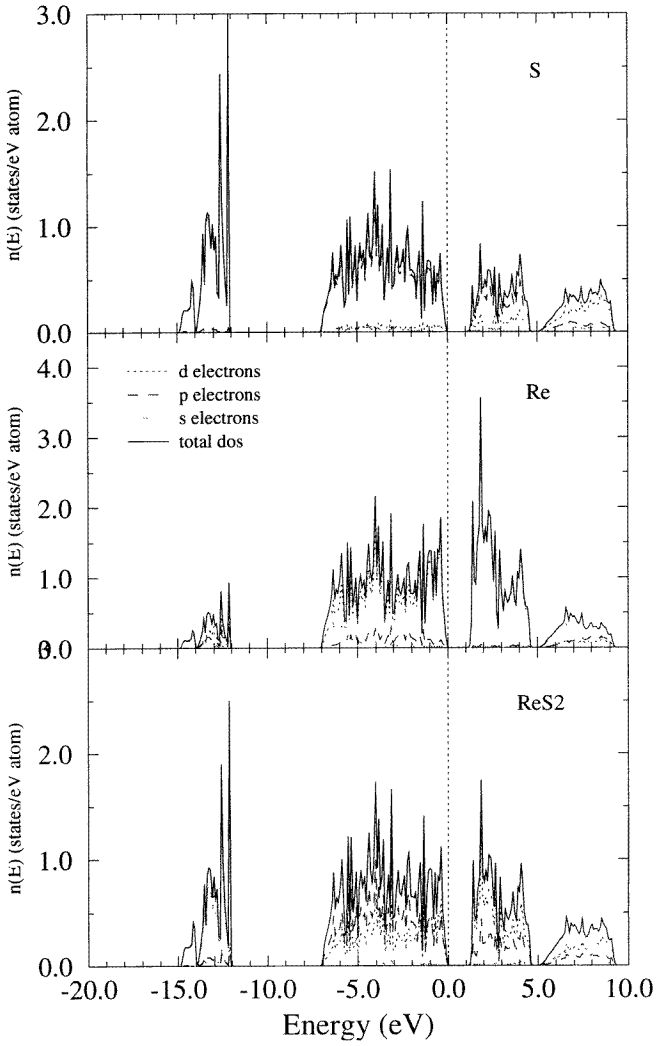

Figure 12. Total and local angular-momentum-decomposed densities of states for triclinic ReS_2 (the key to the curves is the same as in figure 1).

disulphides, magnetic instabilities in CoS_2 and NiS_2, structural instabilities of the heavier IXb disulphides (PdS_2, PtS_2).

4. Electronic structure of the transition-metal monosulphides

4.1. NiAs-type compounds

The total and angular-momentum-decomposed electronic densities of states of the NiAs-type monosulphides from VS to NiS (including a hypothetical MnS phase) are compiled in figure 13. A decomposition into local and partial DOSs is given for the example FeS in figure 14. In accordance with the predominantly ionic character of the compounds, the bands may be arranged into four distinct groups: S 3s bands at $E \sim -15$ to -14 eV, S

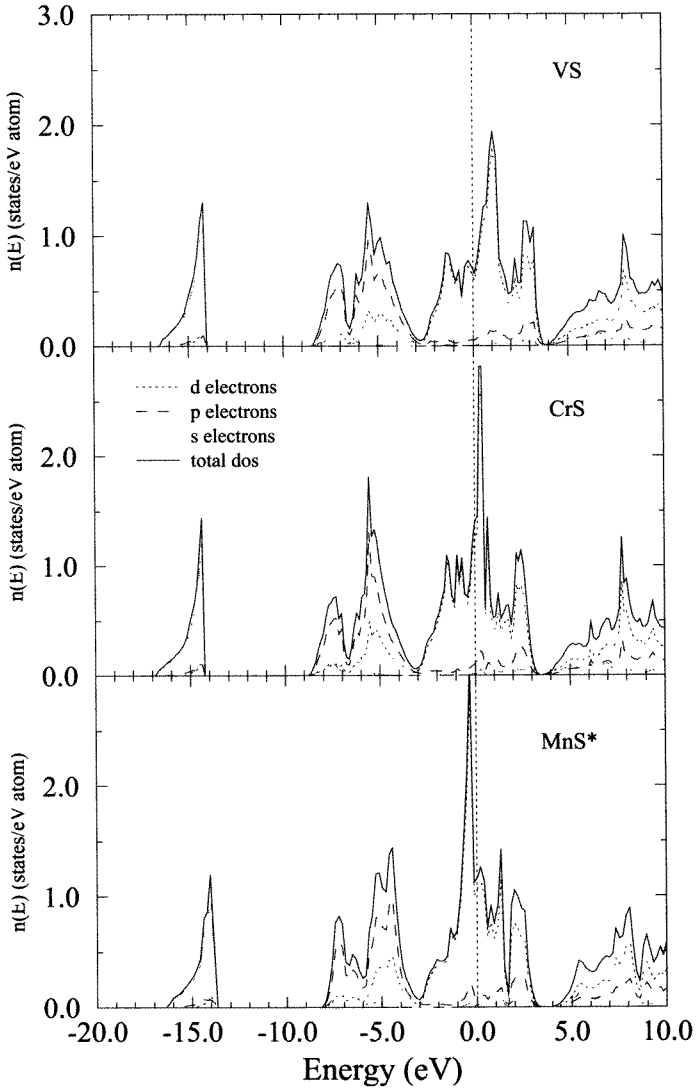

Figure 13. Total and angular-momentum-decomposed electronic densities of states of the 3d monosulphides with the NiAs structure (the key to the curves is the same as in figure 1).

3p bands between −8 eV and −3 eV, overlapping with the TM 3d bands around the Fermi level, and a conduction band at energies >4 eV made up by TM 4s, p and S 3d states. The most important points are the degree of covalent TM d–S p bonding and the structure of the TM d band.

In the NiAs structure the transition-metal atoms are centred in distorted octahedra formed by the S atoms (see I for crystallographic details). Face-sharing octahedra are stacked along the hexagonal axis such that chains of metal atoms are formed. In the octahedral ligand field the d-band manifold splits into triply degenerate t_{2g} and doubly degenerate e_g sets (cf. section 3). Hence some similarity with the layered disulphide compounds with octahedral coordination is expected. However, because of the chain-like arrangement of the

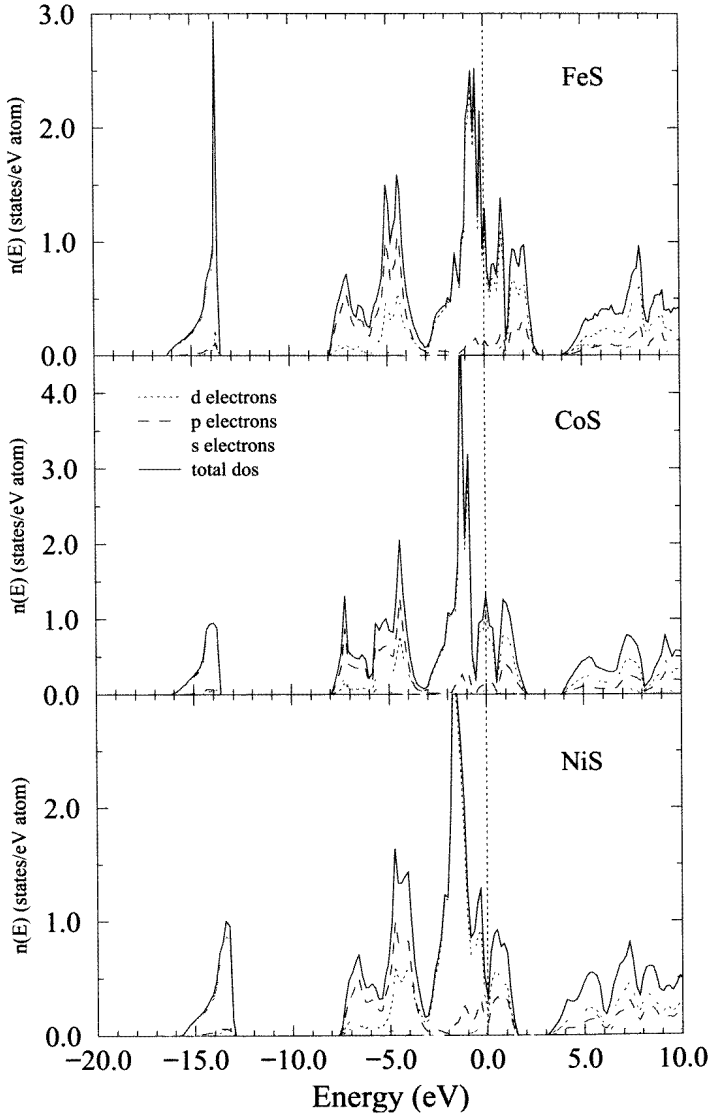

Figure 13. (Continued)

TM atoms, the $d_{3z^2-r^2}$ orbitals show appreciable overlap. Consequently the $d_{3z^2-r^2}$ states are not non-bonding (as is sometimes suggested [29, 35]), but form a broad band that tends to obscure the ligand-field splitting.

The distance ΔE_{p-d} between the highest peaks in the S 3p and TM 3d bands (which is a measure for the ionicity or covalency of the bonding) decreases from $\Delta E_{p-d} \sim 6.5$ eV in VS to $\Delta E_{p-d} \sim 3$ eV in NiS, indicating an increasingly covalent character with increasing filling of the d band. The S p–TM d mixing is also reflected by a substantial contribution of antibonding S 3p states to the DOS at the upper edge of the d band. For CrS, MnS and FeS the Fermi level falls very close to the main peak in the d band. This indicates the instability of the paramagnetic state with respect to the formation of a high-moment antiferromagnetic

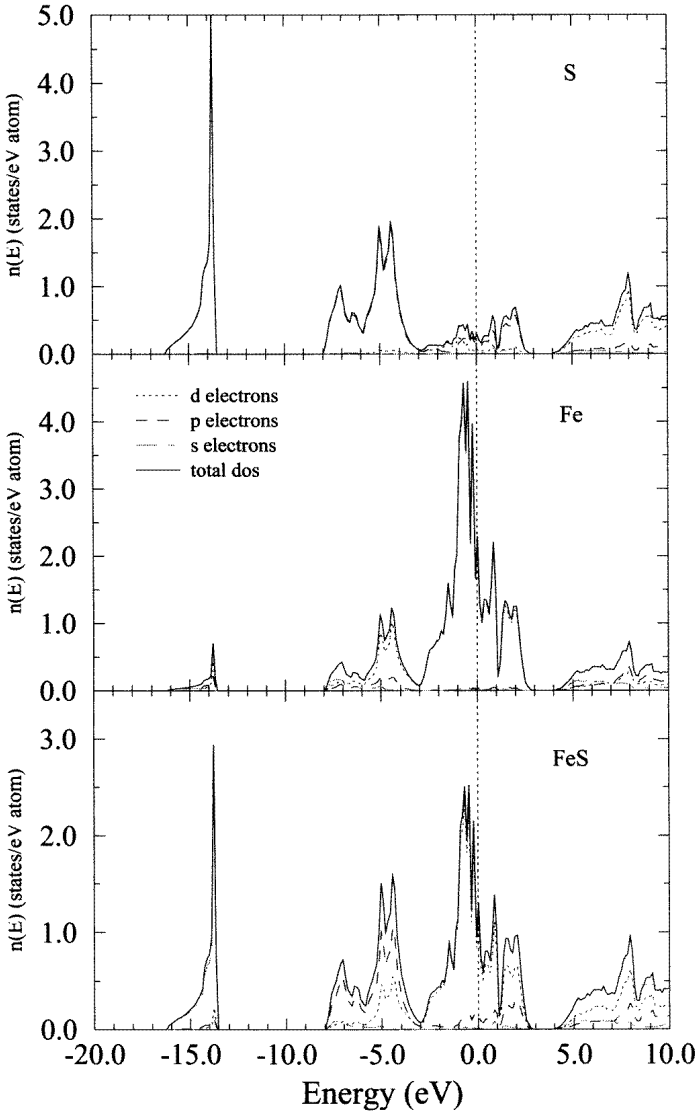

Figure 14. Total, local and partial electronic densities of states of NiAs-type FeS (the key to the curves is the same as in figure 1).

state ($\mu_{Cr} \sim \pm 2.6\ \mu_B$ for CrS, $\mu_{Fe} = \pm 4\ \mu_B$ for FeS). For CoS the Fermi level falls at a secondary maximum of the d-band DOS, resulting in a lower exchange splitting and a lower AFM moment ($\mu_{Co} = \pm 1\ \mu_B$). For NiS the Fermi level falls at a minimum of the DOS—this is like the case for the NaCl-type MnS and NiO compounds which display a DOS minimum at E_F in the paramagnetic state and an insulating gap in the antiferromagnetic state [60]. That the electronic structure of NiS hardly varies across the magnetic ordering transition is confirmed by the recent photoemission measurements of Fujimori *et al* [38, 39]. Figure 15 compares the ultraviolet photoemission spectra with the paramagnetic DOS. The variation of the photoemission intensities with the energy of the incident photons is due

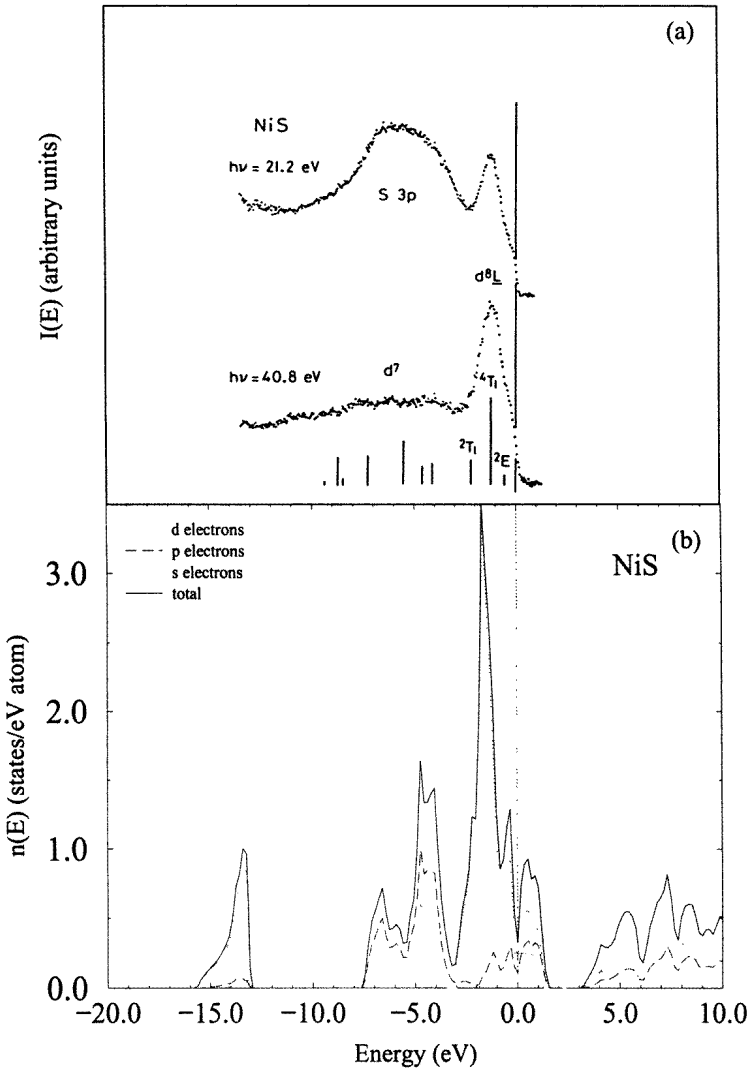

Figure 15. Comparison of the total and partial Ni and S densities of states with the ultraviolet photoemission spectra measured by Fujimori *et al* (reference [39]) at different photon energies. See the text. The vertical bars show the eigenstates for a NiS_6 cluster, calculated by Fujimori *et al.*

to the Cooper minimum in the S 3p photoionization cross-section at $\bar{h}\omega \sim 50$ eV which suppresses the contribution from the partial S 3p DOS [52]. Hence the photoemission spectra confirm the calculated band structure of the paramagnetic phase in detail.

Among the 4d and 5d transition metals, only Nb forms a stable monosulphide with the NiAs structure. Monosulphides with different crystal structures are formed only at the ends of both series (PdS, PtS—see below). The electronic structure of the NiAs-type 4d monosulphides differs from that of the isostructural 3d compounds only by a modest broadening of all sub-bands. This means that for all monosulphides with an approximately half-filled d band the Fermi level falls close to a dominant maximum in the DOS (Cr to Fe in

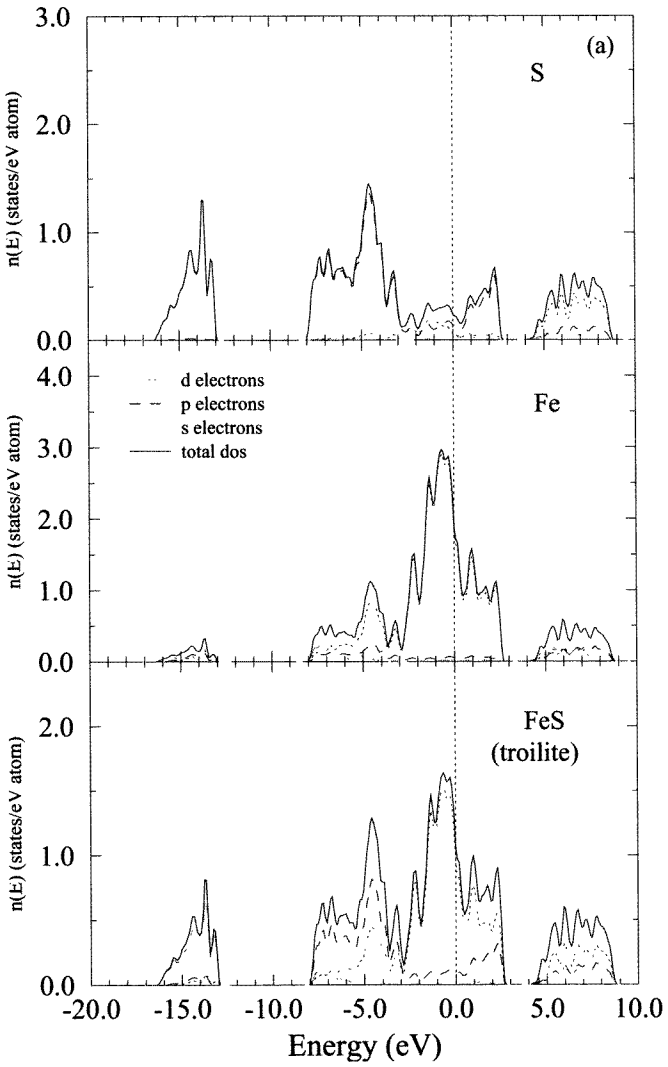

Figure 16. Total, local and partial electronic densities of states in troilite (FeS) (a) and millerite (NiS) (b). The key to the curves is the same as in figure 1.

the 3d series, Mo to Ru in the 4d series). This is intrinsically an energetically unfavourable situation. In the 3d monosulphides the total energy is lowered by the magnetic exchange splitting. In the 4d monosulphides the band broadening reduces the DOS at the Fermi level sufficiently that a magnetic contribution towards the stabilization of the NiAs phase is suppressed.

4.2. Low-temperature phases of the 3d monosulphides

In addition to the NiAs phases of FeS, CoS and NiS, we have also studied the stable low-temperature phases: FeS in the hexagonal troilite structure, NiS in the trigonal millerite

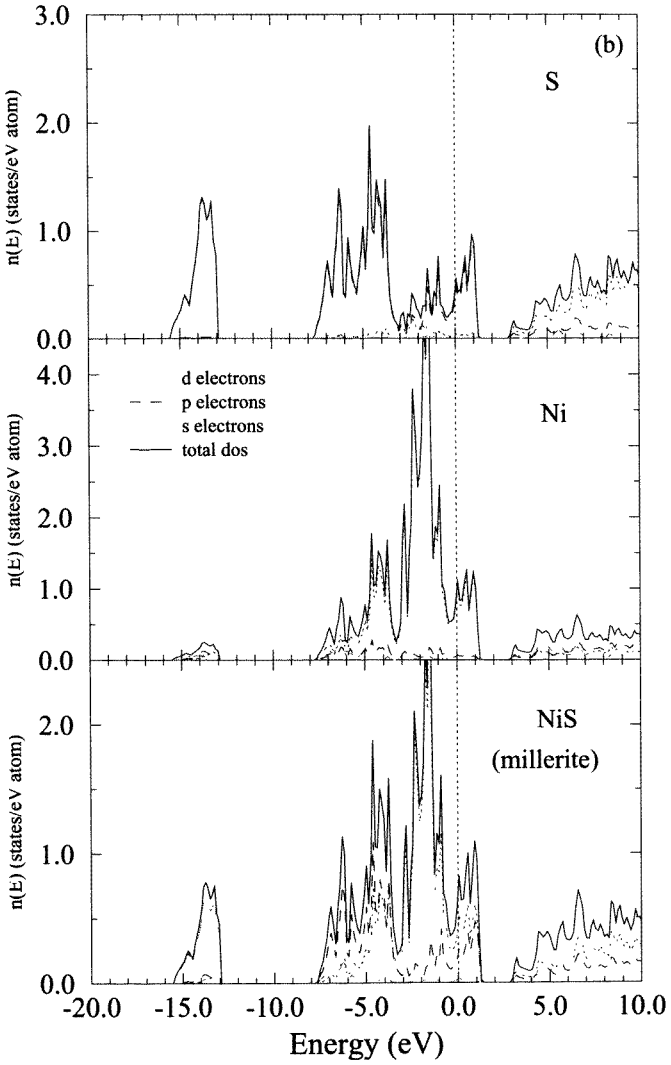

Figure 16. (Continued)

structure and the slightly off-stoichiometric Co_9S_8 phase with a complex cubic structure. A distinctive feature of all three structures is the formation of direct metal–metal contacts. The hexagonal structure of troilite may be considered as a distorted superstructure of the NiAs lattice (see table 1 in I for crystallographic details) where each TM atom has on average four TM nearest neighbours in addition to the six S neighbours. The trigonal structure of millerite can be described in terms of triangular nets of Ni and S alternating along the *c*-direction. The average TM–S and S–TM coordination is reduced from six to five (compared to the NiAs structure), but there are now two direct TM–TM neighbours.

In troilite the closer Fe–Fe coordination leads to a slight broadening of all of the bands and to an increased S 3p–Fe 3d overlap (see figure 16(a)). Due to the distortion of the Fe octahedra and to the stronger Fe–Fe interaction, the ligand-field splitting of the Fe 3d states

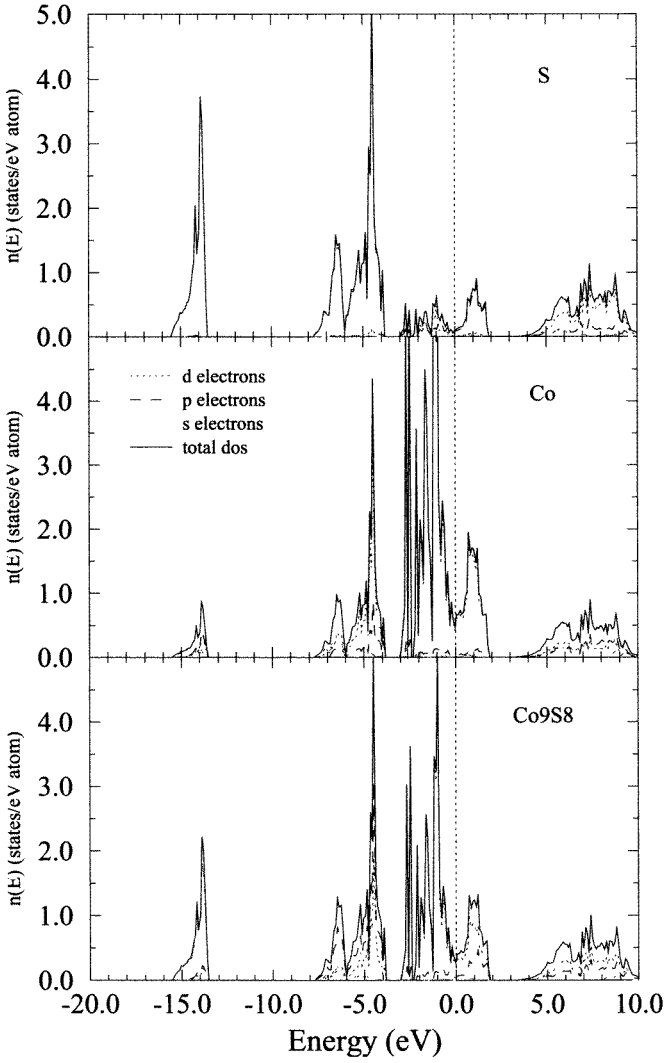

Figure 17. Total, local and partial electronic densities of states in cubic Co_9S_8. The key to the curves is the same as in figure 1.

is quite strongly smeared out. The broadening of the Fe 3d band increases the binding energies of some of the e_g states and this is the main reason for the stabilization of troilite over the NiAs-type phase (by $\Delta E \lesssim 0.01$ eV/atom; cf. table 8 in I). The DOS at the Fermi energy is slightly reduced compared to that of NiAs at high temperature ($n(E_F) = 1.21$ states eV^{-1}/atom).

Comparing the densities of states of millerite (figure 16(b)) with that of the NiAs-type high-temperature phase (see figure 13) we find that the width of the pseudogap at ~ -3.5 eV separating the S 3p and Ni 3d band complexes is reduced, whereas the width of the t_{2g}/e_g pseudogap at the Fermi level is increased. The slight shift of the Ni t_{2g} states to lower energies results from the existence of direct metal–metal neighbours and is the main reason for the energetic stabilization of millerite.

The cubic structure of Co_9S_8 may be considered as a close-packed array of sulphur atoms, with the Co atoms lying at the centres of half of the tetrahedral holes and one eighth of the octahedral holes. Note that relative to that of the monosulphide, the structure contains an excess of metal atoms. Hence the bonding is expected to be different from that in metal-deficient substoichiometric sulphides describable in terms of ordered arrays of vacancies on the NiAs lattice (e.g. Cr_2S_3; see below). The complex structure is described quite accurately in the GGA (see I). The octahedrally coordinated Co atoms have six S neighbours; the tetrahedrally coordinated Co atoms have four nearest S neighbours plus three S atoms at a distance that is only 0.009 Å larger and three Co neighbours (see table 1 in I). The S atoms are tetrahedrally coordinated by four Co atoms (plus at some sites an extra Co neighbour). The mixed character of the Co–S coordination leads to a profound modification of the electronic spectrum (see figure 17): instead of falling at a local maximum of the DOS as for NiAs-type CoS, the Fermi level now falls at a deep pseudogap between the lower part of the Co 3d band (which has only a weak interaction with the S 3p band) and the upper part, showing appreciable hybridization with the S 3pσ^* states. The reduced S–S coordination also leads to a narrowing of the S 3pπ, pπ^*, pσ band complex which is separated from the Co 3d band. Hence the stabilization of the Co_9S_8 phase results mainly from the formation of the structure-induced pseudogap at E_F (for the energetics, see table 8 and figure 4(b) in I).

4.3. PdS and PtS

Among the 4d and 5d metals only Pd and Pt form stable monosulphides, albeit with quite different crystal structures. In the tetragonal PtS structure the S atoms occupy the corners of a simple tetragonal cell (axial ratio $c/a = 1.76$), while the Pt atoms lie at the centres of two opposite faces, alternatingly, in the (100) direction. Hence like-atom bonds are formed only parallel to the (x, y) plane, in the form of d(t_{2g})–π and p_x, p_y, p_z–π bonds between the S and TM atoms. Unlike-atom bonds are formed by linear combinations of p_z, d_{xy} and p_z, d_{yz} orbitals in alternating rows. The $d_{3z^2-r^2}$ orbitals remain essentially non-bonding. Compared to the band structure of NiAs-type NiS, the main differences are a weak bonding–antibonding splitting in the low-lying S 3s band and the increased bonding–antibonding splitting in the S 3pσ–TM ($d_{t_{2g}} + d_{x^2-y^2}$) band complex (see figure 18(a)). The Fermi level falls at a very deep DOS minimum (essentially a zero-energy gap) at the upper edge of the non-bonding $d_{3z^2-r^2}$ band.

PdS forms a complex tetragonal structure which is most often described in terms of alternating hexagon–triangle and square–triangle nets occupied by Pd and S atoms respectively. As in PtS, the Pd atoms lie at the centres of a planar arrangement of four neighbours (see I for detailed references). The electronic density of states (see figure 18(b)) indicates that as in the case of PtS—and as for the low-temperature phases of NiS and FeS—the formation of a deep pseudogap at the Fermi level is the driving electronic mechanism for the stabilization of the Pd and Pt monosulphides.

5. Sulphides of other stoichiometries

As representative examples for TMS with other stoichiometries we have considered Cr_2S_3 (whose crystal structure may be interpreted as an ordered defect superstructure of NiAs), Rh_2S_3 and Ni_3S_2 (essentially filled-up derivatives of a body-centred cubic packing). The comparison of the density of states of Cr_2S_3 (see figure 19) with that of NiAs-type CrS (see figure 13) shows that the introduction of vacancies leaves the overall form of the DOS

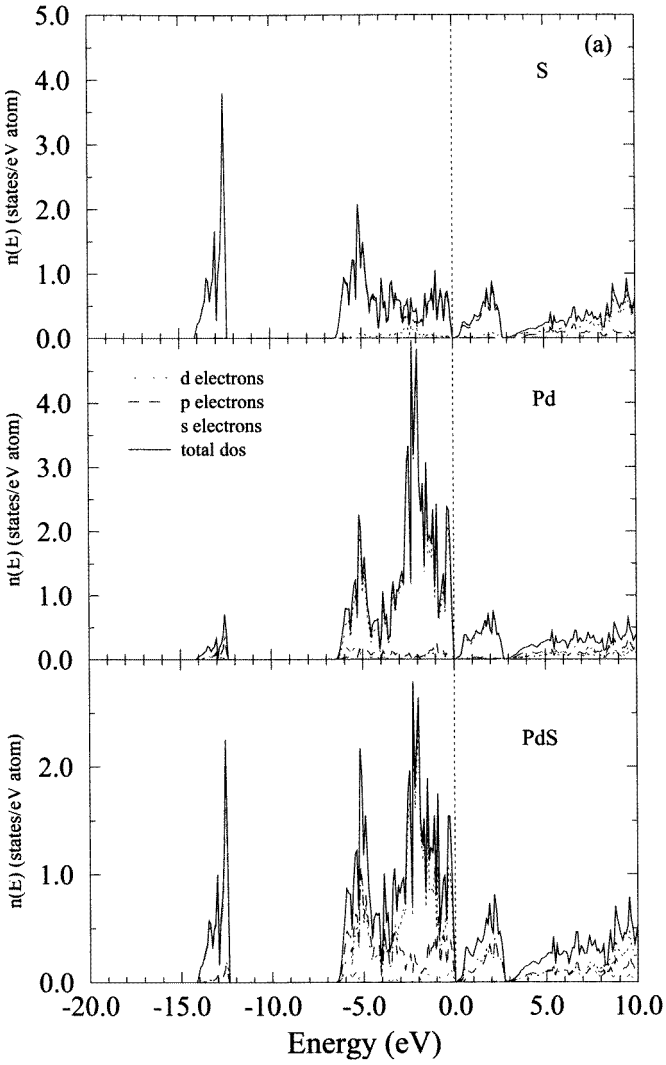

Figure 18. Total, local and partial electronic densities of states in hexagonal PdS (a) and in trigonal PtS (b). The key to the curves is the same as in figure 1.

essentially unchanged. The reason for this is that as in the NiAs structure the S atoms in Cr_2S_3 form hexagonal close-packed layers, with layers of Cr atoms occupying alternately all and one third of the octahedral holes in the S network. Hence the octahedral coordination of the TM atoms remains the determining factor for the structure of the Cr 3d band. Because of the reduced Cr concentration the occupation of the essentially non-bonding Cr $d_{3z^2-r^2}$ band close to the Fermi level is reduced (this band contributes mainly to the Cr–Cr bonds). The DOS at the Fermi level is reduced relative to that of CrS, but remains sufficiently high to destabilize the paramagnetic state against ferromagnetic ordering. Our results for the band structure of Cr_2S_3 are similar to the results of Dijkstra *et al* [35] for the substoichiometric selenides and tellurides of Cr.

The crystal structure of Rh_2S_3 contains pairs of face-sharing distorted octahedra of

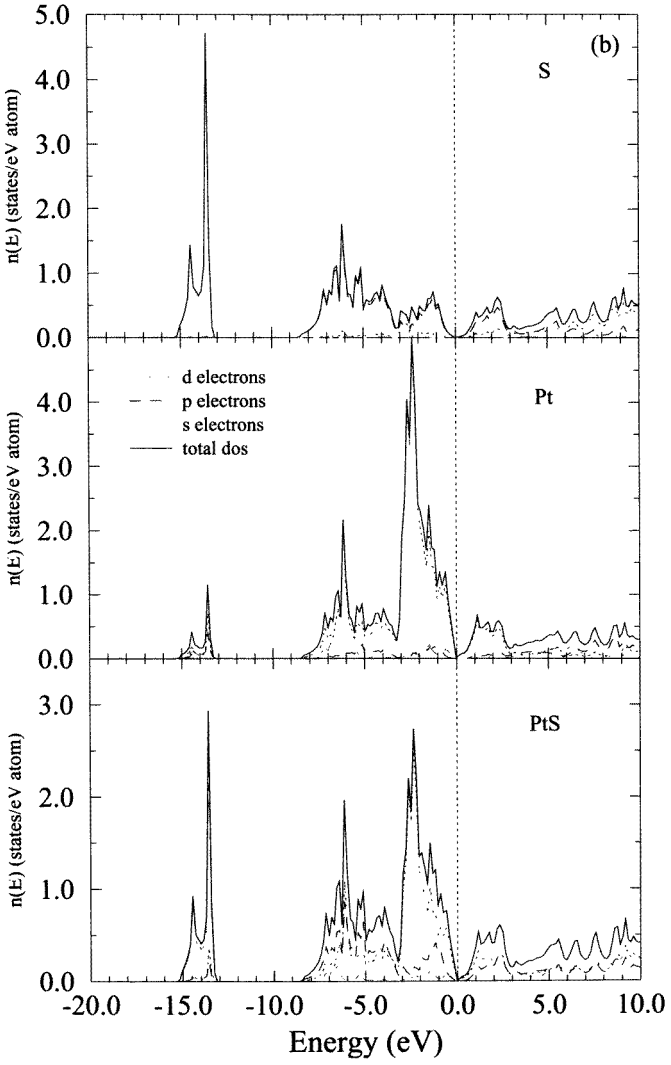

Figure 18. (Continued)

S surrounding Rh. The S atoms have four Rh neighbours forming a strongly distorted tetrahedron. The electronic structure turns out to be dominated by the splitting of the Rh 4d band into t_{2g} and e_g manifolds induced by the distorted octahedral ligand field (similarly to in the pyrite structure); see figure 20. Due to the reduced Rh concentration, the Fermi level falls in the t_{2g}/e_g gap ($E_g = 0.09$ eV). However, the distortion of the octahedral environment leads to relatively short Rh–Rh distances across the common triangular face of the octahedra, so the t_{2g} orbitals are no longer completely non-bonding but interact considerably with the S 3p states.

In trigonal Ni_3S_2 the S atoms form a slightly distorted body-centred cubic array with the Ni atoms at the centre of distorted tetrahedral holes arranged in such a way that they form spirals running along the hexagonal axis. Besides the tetrahedrally arranged S atoms, each Ni atom has four Ni neighbours at distances that are only ∼0.2 Å larger than the NiS

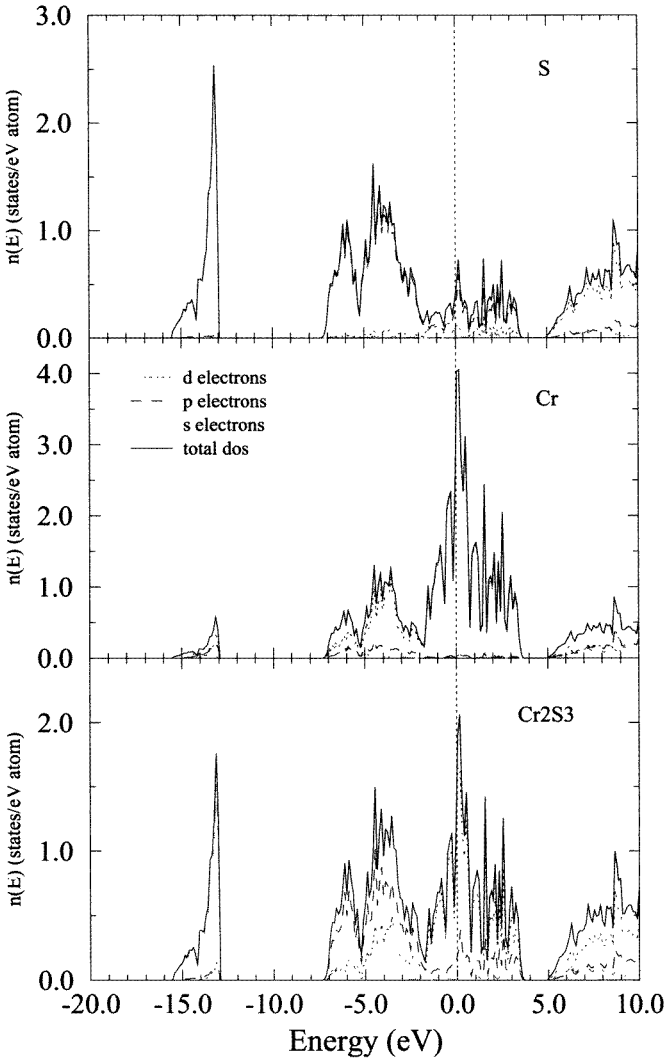

Figure 19. Total, local and partial electronic densities of states in trigonal Cr_2S_3. The key to the curves is the same as in figure 1.

distances. The calculated DOS (see figure 21) shows an overall similarity to that of the two NiS polymorphs, with the Fermi level separating the Ni orbitals interacting with the S $3p\sigma^*, \pi$ band complex from the Ni 3d band.

6. Electronic structure versus catalytic activity

We are now in a position to return to one of the initial motivations of this study, i.e. a possible correlation between the electronic structure of the TMS and their activity as catalysts in hydro-desulphurization (HDS) reactions. In their studies of HDS activities of TMS, Harris and Chianelli [61] and more recently Toulhoat *et al* [62] pointed to a correlation between a high HDS activity and an intermediate TM–S bond strength or heat of formation, in the spirit

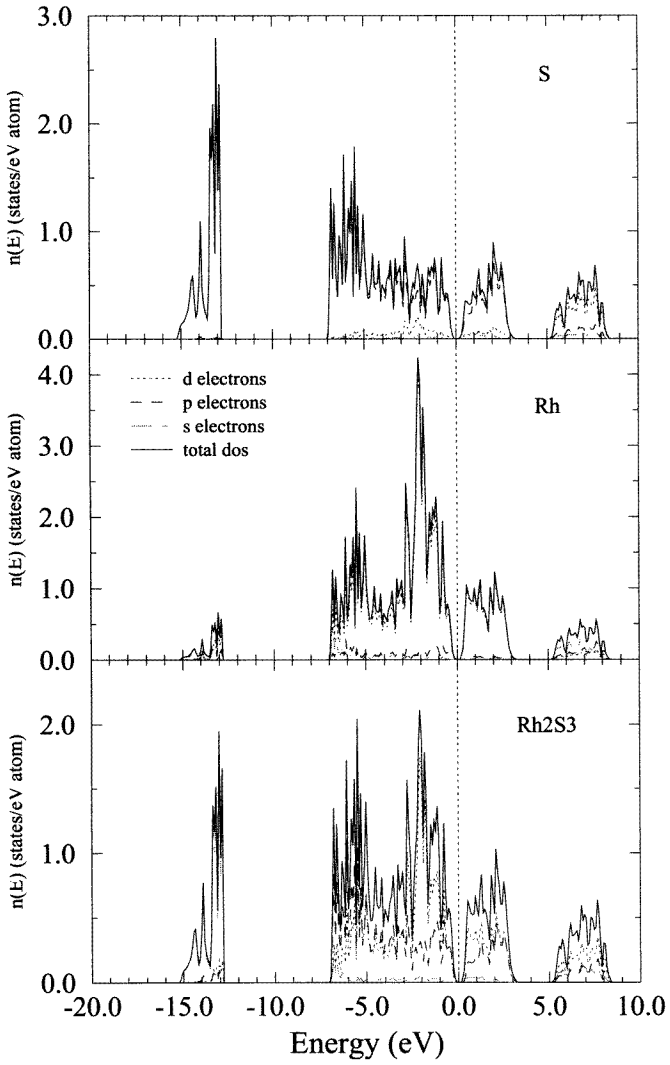

Figure 20. Total, local and partial electronic densities of states in orthorhombic Rh_2S_3. The key to the curves is the same as in figure 1.

of the principle of Sabatier [63]. In addition, Harris and Chianelli attempted to establish on the basis of LDF cluster-calculation correlations between HDS activity and electronic properties. One factor identified in their study was the ability of the TM to bond covalently, via σ or π bonds, to the 3p orbitals of sulphur. Covalency was measured in terms of the metal contributions to the bonding $2e_g(\sigma)$ and $1t_{2g}(\pi)$ TM–S states of an octahedral TM S_6^{n-} cluster. The second factor is the number of TM d electrons in the highest occupied molecular orbital (HOMO). In addition it was found that for the most active catalysts the HOMO is the $2t_{2g}$ orbital. The interpretation of these correlations is based on the fact that one step in the catalytic process must be the bonding of the sulphur-containing molecule (e.g. thiophene or benzothiophene) to the catalyst surface through a metal atom exposed by the formation of a sulphur vacancy. The ability of the TM atoms to form a strong covalent

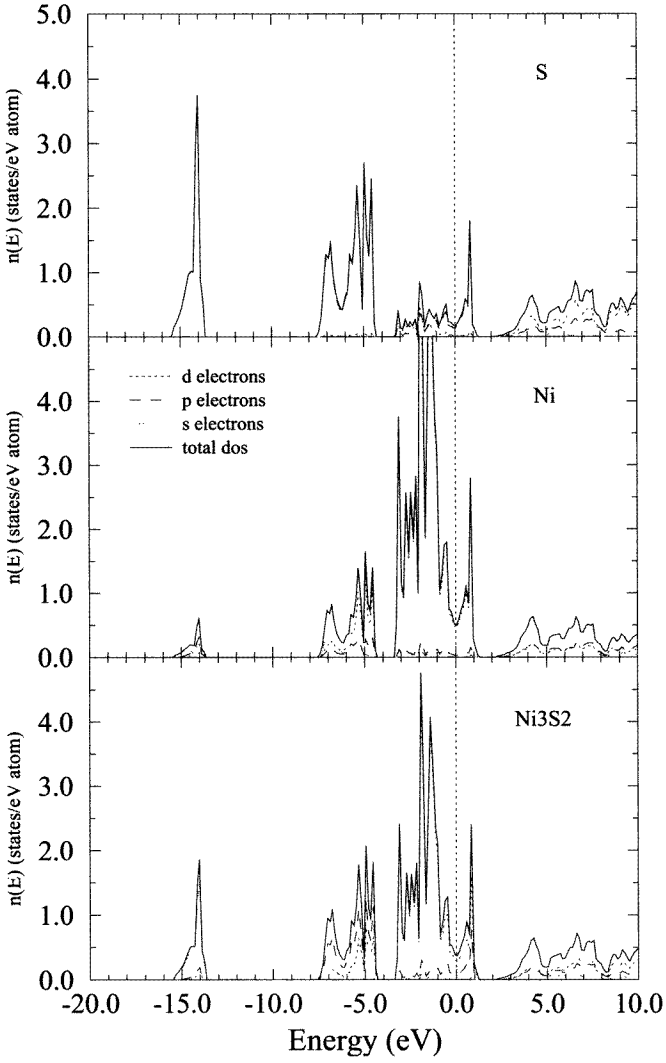

Figure 21. Total, local and partial electronic densities of states in trigonal Ni_3S_2. The key to the curves is the same as in figure 1.

bond with the sulphur atom in the thiophene ring could be a determining factor in the adsorption process—if the molecule does indeed bind to the surface through a strong TM–S bond. The correlation with the number of d electrons in the HOMO (or equivalently with the density of states at the Fermi level of the bulk TMS) was interpreted in a similar spirit in terms of the ability of the TMS to back-donate electrons to the ring sulphur. π back-donation from the two t_{2g} levels to the antibonding π^* orbitals of the ring was considered as particularly effective because it contributes to the weakening of the carbon–sulphur bond that must ultimately be broken in the HDS process. However, Harris and Chianelli [61] also emphasized that it remains to be seen how well the cluster model correlates with the actual electronic structure of the TMS and in particular with the surface electronic structure.

If we order the TMS covered in this study with respect of their HDS activity (see

Table 1. Transition-metal sulphides ranked according to their catalytic activity for hydrodesulphurization, together with the width of the semiconducting band gap and the symmetry of the highest occupied molecular orbital.

Compound/structure	HDS activity[a]	Band gap (eV)	Symmetry of the HOMO
RuS_2/pyrite	4×10^{18}	0.56	t_{2g}
OsS_2/pyrite	2×10^{18}	0.11	t_{2g}
Rh_2S_3/Rh_2S_3	1×10^{18}	0.09	t_{2g}
Ir_2S_3/Rh_2S_3	1×10^{18}		t_{2g}
ReS_2/ReS_2	4×10^{17}	1.17	$a_{1g}(d_{xy}, d_{x^2-y^2})$
PtS/PtS	2×10^{17}	$\lesssim 0.05$	
PdS/PdS	1×10^{17}	$\lesssim 0.05$	
MoS_2/layered	8×10^{16}	0.89	$a_{1g}(d_{3x^2-r^2})$
WS_2/layered	4×10^{16}	0.91	$a_{1g}(d_{3x^2-r^2})$
NbS_2/layered	1×10^{16}	Metallic	
TaS_2/layered	1×10^{16}	Metallic	

[a] Measured in molecules of dibenzothiophene converted per second and millimole of metal in the catalyst. After Pecoraro and Chianelli, reference [64].

table 1) we find that all TMS with a substantial catalytic activity are semiconducting. With the sole exception of FeS_2, all of the TMS comply with this correlation in the inverse direction also: all semiconducting TMS are HDS active. The failure of FeS_2 (both pyrite and marcasite) to comply with this rule is probably related to the low stability of FeS_2 under the conditions of the catalytic reaction rather than to an intrinsic absence of HDS activity (Pecoraro and Chianelli [64] do not offer a more precise characterization of the TMS on which the measurements of the activity have been performed).

As the opening of a band gap in the DOS of the TMS is always the consequence of a strong bonding–antibonding splitting in the S $3p\pi$–TM d band complex, the correlation between semiconducting behaviour and high HDS activity simply re-expresses the importance of a strong covalent contribution to the metal–sulphur bond (as already noted by Harris and Chianelli [61]).

There is, however, no evident correlation with the width of the optical gap: Rh_2S_3 and Ir_2S_3 with a very narrow gap of $\sim$0.09 eV are more active than MoS_2 and WS_2 with a gap of almost 1 eV. More important seems to be the character of the states in the highest occupied valence bands: the highest HDS activity is found in the pyrite compounds RuS_2 and OsS_2 where the highest occupied band is the non-bonding TM t_{2g} (d_{xy}, d_{yz}, d_{xz}) band formed as a consequence of the ligand-field splitting of the d levels in an octahedral environment. In the semiconducting layered compounds with trigonal-prismatic TM environments (MoS_2, WS_2), the highest occupied band split from the t_{2g} triplet has a_{1g} symmetry (i.e. mostly $d_{3z^2-r^2}$ character in a coordinate system oriented along the hexagonal axis)—this corresponds to a lower HDS activity. In ReS_2 the structural distortion of the octahedral environment leads to a Jahn–Teller splitting of the t_{2g} band complex. Hence the increasing occupation of the t_{2g} band complex (1/3 in MoS_2/WS_2, 1/2 in ReS_2, 1 in RuS_2/OsS_2) correlates with an increasing HDS activity. The remaining HDS-active TMS also fit into this scheme: in Rh_2S_3 and Ir_2S_3 the Fermi level falls in the t_{2g}/e_g gap produced by the distorted octahedral ligand field—corresponding again to a high activity. In PdS and PtS the TM d band is 80% filled, according to simple valence rules. In both structures the TM atoms lie at the centre of a planar arrangement of 4s atoms, so the largest bonding–antibonding splitting occurs between states formed by S ($p_z + p_x$) and TM d_{xz} states (and similar yz-linear

combinations). The occupied states show appreciable non-t_{2g} admixture—corresponding to lower HDS activity. However, if this really corresponds to an increasing ability of the t_{2g} states to back-donate the antibonding π^* C–S states in an adsorbed heterocyclic molecule remains to be clarified by detailed calculations of the surface electronic structure—evidently the orientation of the exposed surface will be important.

7. Conclusions

Our investigations extend and confirm earlier studies that had suggested that the electronic structure of the TMS is determined largely by short-range interactions in the S 3p–TM d band complex and in particular by the ligand-field splitting of the TM d states in the (eventually distorted) octahedral or trigonal environment of S atoms. In particular we show that the trend from layered disulphides through triclinic ReS_2 and TcS_2 to pyrite-type disulphides with increasing filling of the d band is a consequence of the d-band splitting—the most stable structure is always the one for which all of the states below the largest gap in the d band are filled. Semiconducting properties are predicted for layered MoS_2 and WS_2, for ReS_2 and for the pyrites of the Fe-group metals. Strong covalent bonding and the formation of a structure-induced gap or pseudogap (=the DOS minimum) at the Fermi level are also important for understanding the stability of the late 4d and 5d monosulphides (PdS, PtS), of substoichiometric sulphides such as Co_9S_8, and of sulphides of intermediate stoichiometry (e.g. Cr_2S_3) that can be interpreted as defect NiAs-type phases.

Our new results also lead to a clearer picture of the correlation between the electronic structure and catalytic activity for hydro-desulphurization: all TMS with a high HDS activity are semiconducting and tend to have a high degree of t_{2g} character in the highest occupied orbitals.

Acknowledgments

This work was performed within the Groupement de Recherche Européen ‘Dynamique moléculaire quantique appliquée à la catalyse, à l’adsorption et à l’absorption’, supported by the Institut Français du Pétrole and the Centre National de la Recherche Scientifique (France).

References

[1] Raybaud P, Kresse G, Hafner J and Toulhoat H 1997 *J. Phys.: Condens. Matter* **9** 11 085
[2] Kohn W and Sham L J 1964 *Phys. Rev.* **140** A1133
Kohn W 1985 *Highlights of Condensed Matter Theory* ed M P Tosi and F Bassani (Amsterdam: North-Holland)
[3] Jones R O and Gunnarsson O 1989 *Rev. Mod. Phys.* **61** 689
[4] Perdew J P, Chevary J A, Vosko S H, Jackson K A, Pedersen M R, Singh D J and Fiolhais C 1992 *Phys. Rev.* B **46** 6671
[5] Wilson J A and Yoffe A D 1969 *Adv. Phys.* **18** 193
[6] Huisman R, de Jonge R, Haas C and Jellinek F 1971 *J. Solid State Chem.* **3** 56
[7] Mattheis L F 1973 *Phys. Rev.* B **8** 3719
[8] Bullett D W 1978 *J. Phys. C: Solid State Phys.* **11** 4501
[9] Hughbanks T and Hoffmann R 1984 *J. Am. Chem. Soc.* **105** 1150
[10] Kertesz M and Hoffmann R 1986 *J. Am. Chem. Soc.* **106** 3453
[11] Coehoorn R, Haas C, Dijkstra J, Flipse C J F, de Groot R A and Wold A 1987 *Phys. Rev.* B **35** 6195
[12] Li E K, Johnson K H, Eastman D E and Freouff J L 1974 *Phys. Rev. Lett.* **32** 470
[13] Tossel J A 1977 *J. Chem. Phys.* **66** 5712

Tossel A, Vaughan D J and Burdett J K 1977 *Physics and Chemistry of Minerals* vol 7 (Berlin: Springer) p 177
[14] Khan H A 1974 *J. Phys. C: Solid State Phys.* **9** 81
[15] Bullett D W 1982 *J. Phys. C: Solid State Phys.* **15** 6163
[16] Wilson J A and Pitt G D 1971 *Phil. Mag.* **23** 1297
Wilson J A 1985 *The Metallic and Non-metallic States of Matter* ed P P Edwards (London: Taylor and Francis)
[17] Lauer S, Trautwein A X and Harris F E 1984 *Phys. Rev.* B **29** 6774
[18] Kuhne H M, Jägermann W and Tributsch H 1984 *Chem. Phys. Lett.* **112** 160
[19] Holzwarth N A W, Harris S and Liang K S 1985 *Phys. Rev.* B **32** 3745
[20] Folkerts W, Sawatzky G A, Haas C, de Groot R A and Hillebrecht F V 1987 *J. Phys. C: Solid State Phys.* **20** 4135
[21] Zhao G L, Callaway J and Hayashibara M 1993 *Phys. Rev.* B **48** 15 781
[22] Zeng Y and Holzwarth N A W 1994 *Phys. Rev.* B **50** 8214
[23] Matsuura A Y, Shen Z X, Dessau D S, Park C H, Thio T, Bennett J W and Jepsen O 1996 *Phys. Rev.* B **53** R7584
[24] Huang Y S and Chen Y F 1988 *Phys. Rev.* **38** 7997
[25] Muro T, Shishido T, Oda F, Fukawa T, Yamada H, Kimura A, Imida S, Suga S, Park S Y, Miyahara T and Sato K 1996 *Phys. Rev.* B **53** 7055
[26] Bocquet A E, Mamiya K, Mizokawa T, Fujimori A, Miyadai T, Takahashi H, Mori M and Suga S 1996 *J. Phys.: Condens. Matter* **8** 2389
[27] Sparks J T and Komoto T 1967 *Phys. Lett.* **25A** 398
[28] Barker A S and Remeika J P 1974 *Phys. Rev.* B **10** 987
[29] White R M and Mott N F 1971 *Phil. Mag.* **24** 845
[30] Wilson J A 1972 *Adv. Phys.* **21** 143
[31] Tyler J M and Fry J L 1970 *Phys. Rev.* B **1** 4604
[32] Mattheis L F 1974 *Phys. Rev.* B **10** 995
[33] Kasowski R V 1973 *Phys. Rev.* B **8** 1378
[34] Motizuki K, Kotoh K and Yamase A 1986 *J. Phys. C: Solid State Phys.* **19** 495
[35] Dijkstra J, van Bruggen C F, Haas C and de Groot R A 1989 *J. Phys.: Condens. Matter* **1** 9163
[36] Podloucky R 1984 *Solid State Commun.* **50** 763
[37] Coehoorn R, Haas C and de Groot R A 1995 *Phys. Rev.* B **31** 1980
[38] Fujimori A, Terakura K, Taniguchi M, Ogana S, Suga S, Matoba M and Anzai S 1988 *Phys. Rev.* B **37** 3109
[39] Fujimori A, Namabame H, Matoba M and Anzai S 1990 *Phys. Rev.* B **42** 620
[40] Kresse G and Furthmüller J 1996 *Comput. Mater. Sci.* **6** 15
Kresse G and Furthmüller J 1996 *Phys. Rev.* B **54** 11 169
[41] Schlegel A and Wachter P 1976 *J. Phys. C: Solid State Phys.* **9** 3363
[42] Bichsel R, Levy F and Berger H 1984 *J. Phys. C: Solid State Phys.* **17** L19
[43] van der Heide H, Hemmel R, van Bruggen C and Haas C 1980 *J. Solid State Chem.* **33** 17
[44] Bocquet A E, Mamiya K, Mizokawa T, Fujimori A, Miyadai T, Takahashi H, Mori M and Suga S 1996 *J. Phys.: Condens. Matter* **8** 2389
[45] Fujimori A, Mamiya K, Mizokawa R, Miyadai T, Sekiguchi T, Takahashi H, Mori N and Suga S 1996 *Phys. Rev.* B **54** 16 329
[46] Benoit R 1955 *J. Chim. Phys.* **52** 119
[47] Korenman V and Prange A E 1979 *Phys. Rev.* B **19** 4691
[48] Zaanen J, Sawatzky G A and Allen J W 1985 *Phys. Rev. Lett.* **55** 418
[49] Ballhausen C J 1962 *Introduction to Ligand Field Theory* (New York: McGraw-Hill)
[50] Abbati I, Braicovich L, Carbone C, Nogami J, Lindau I and del Pennino U 1986 *J. Electron Spectrosc. Relat. Phenom.* **40** 353
[51] Cooper J W 1964 *Phys. Rev. Lett.* **13** 762
[52] Yeh J J and Lindau I 1985 *At. Data Nucl. Data Tables* **32** 1
[53] Li C H and Tong S V 1972 *Phys. Rev. Lett.* **42** 901
[54] Šimunek A and Wiech G 1984 *Phys. Rev.* B **30** 923
[55] Haycock D E, Urch D S and Wiech G 1979 *J. Chem. Soc. Faraday Trans.* II **75** 1692
[56] Li Dien, Bancroft G M, Kasrai M, Fleet M E, Feng X H and Tan K H 1995 *Phys. Chem. Minerals* **22** 123
[57] Wildervanck J C and Jellinek F 1971 *J. Less-Common Met.* **24** 73
[58] See, e.g., the lectures of
di Salvo F J, de Wolf P M *et al* 1977 *Electron–Phonon Interactions and Phase Transitions* ed T Riste (New

York: Plenum)
[59] Markolikas C and Amelinckx S 1980 *Physica* B+C **99** 31
[60] Oguchi T, Terakura K and Williams A R 1983 *Phys. Rev.* B **28** 6443
[61] Harris S and Chianelli R R 1984 *J. Catal.* **86** 400
Harris S and Chianelli R R 1986 *J. Catal.* **98** 17
[62] Toulhoat H, Raybaud P, Kastelan S, Kresse G and Hafner J 1997 *Symp. on Advances and Applications of Computational Chemical Modelling to Heterogeneous Catalysis (San Francisco, CA, 1997)* (New York: American Chemical Society) at press
[63] Sabatier P 1911 *Ber. Deutsch. Chem. Ges.* **44** 1984
[64] Pecoraro T A and Chianelli R R 1981 *J. Catal.* **67** 430